Master's Thesis

Super-concentrated aqueous electrolyte to improve rechargeability of symmetric lithium manganese oxide batteries

Do Sol Cheong

Department of Chemical Engineering

Graduate School of UNIST

2020

Super-concentrated aqueous electrolyte to improve rechargeability of symmetric lithium manganese oxide batteries

Do Sol Cheong

Department of Chemical Engineering

Graduate School of UNIST

Super-concentrated aqueous electrolyte to improve rechargeability of symmetric lithium manganese oxide batteries

A thesis/dissertation
submitted to the Graduate School of UNIST
in partial fulfillment of the
requirements for the degree of
Master of Science

Do Sol Cheong

01. 09. 2020
Approved by

Advisor
Hyun-Kon Song

Super-concentrated aqueous electrolyte to improve rechargeability of symmetric lithium manganese oxide batteries

Do Sol Cheong

This certifies that the thesis/dissertation of Do Sol Cheong is approved.

01. 09. 2020

signature

Advisor: Hyun-Kon Song

signature

typed name: Nam-Soon Choi

signature

typed name: Hochun Lee

Abstract

Graphite coating on lithium manganese oxide (LMO@Gn) enables to use 3 V region reaction of lithium manganese oxide (LMO) with overcoming Jahn-Teller distortion. In this research, 3V region of LMO is used as anode and cathode with its 3 V and 4 V redox to realize 1 V symmetric LMO rocking-chair battery system. Traditional aqueous electrolytes and 21 m LiTFSI aqueous solution (water-in-salt electrolyte, WiSE), conventional carbonate based organic electrolytes were tested in this battery systems. Even though traditional aqueous electrolytes have great kinetic properties, traditional aqueous electrolytes are suffered by poor electrochemical stability based on water decomposition. Organic electrolytes have the best electrochemical stability. However, its low ionic conductivity and low transference number of lithium ion make its kinetic properties poor. WiSE shows the best performance among the candidates with optimized balance between kinetics and electrochemical stability. Through these, symmetric LMO rocking-chair battery system which was failure in previous can be realized. From using WiSE, this symmetric LMO battery system can be operated in low temperature (~-30 ^{o}C), high C rate (10C) with great rechargeability.

Contents

List of Figures

1. Introduction

1.1 Overview

Electric vehicles (EVs) have been popularly available since 1997, the year in which Toyota presented Prius. The first market-meaningful hybrid EV (HEV) adopted nickel metal hydride (Ni-MH) batteries using aqueous alkaline electrolytes.[1] Whereafter, lithium ion batteries (LIBs) using carbonate-based organic electrolytes have replaced the aqueous batteries in EVs due to their high energy densities.[2] The use of organic electrolytes was inevitable to allow the working cell voltages of LIBs to be larger than 3 V even if it possessed the problems of flammability and toxicity of organic solvents. [3] After LIBs conquered the market of energy storage devices for portable electronic devices, EVs and large-scale energy storage systems (ESSs), the concerns on the safety issues mainly triggered by organic electrolytes have increased continuously. Therefore, the batteries based on aqueous electrolytes have been re-considered from the eco-friendly standpoint even if high energy densities of the LIB level were not fully guaranteed. [4]

Presently available aqueous batteries include lead-acid, Ni-Cd and Ni-MH cells. However, their sustainable usage could be guaranteed after overcoming the corrosive hazards of extremely basic or acidic electrolytes (5 to 8 M KOH or 4 to 6 M H_2SO_4)[5, 6], the toxicity of lead (Pb) and cadmium (Cd) and the insecure supply of rare earth elements (La, Nd and Pr) of alloys for electrodes of Ni-MH batteries. Alternatively, rechargeable LIBs based on aqueous electrolytes (ARLB for aqueous rechargeable lithium battery) have been presented. One of the very first works by Dahn group used lithium manganese oxide spinel ($LiMn_2O_4$) as the active materials of both cathode and anode in the presence of the aqueous solution of 5 M $LiNO_3$.[7] The symmetric cell design was possible because $LiMn_2O_4$ is amphi-redox-active.[8] During the charge process of the $LiMn_2O_4||LiMn_2O_4$ cells, $LiMn_2O_4$ on cathode is delithiated at >3.9 V_{Li} (V versus Li/Li^+) (equation 1) while $LiMn_2O_4$ on anode is lithiated at ~2.9 V_{Li} (equation 2):

$LiMn(III)Mn(IV)O_4 \rightarrow Mn(IV)Mn(IV)O_4 + Li^+ + e^-$ at > 3.9 V_{Li} (1)

$LiMn(III)Mn(IV)O_4 + Li^+ + e^- \rightarrow Li_2Mn(III)Mn(III)O_4$ at ~2.9 V_{Li} (2).

However, the symmetric cell operation was totally failed, showing very poor cyclability. [7] Both electrode and electrolyte failure would be responsible for the unsuccessful operation of the $LiMn_2O_4||LiMn_2O_4$ cells. From the electrode standpoint, the additional lithiation of $LiMn_2O_4$ (equation 2) changes the structure from cubic to tetragonal, inducing the Jahn-Teller distortion.[9] The stress developed by the distortion encourages the structural instability of the anode material. Also, the trivalent manganese species in $Li_2Mn(III)Mn(III)O_4$ accelerate the disproportionation reaction to generate divalent species that is easily soluble in electrolyte.

The electrochemical instability of aqueous electrolytes is the second failure. It appears to be inevitable that aqueous electrolytes have an electrochemically stable potential window much narrower than that of organic electrolytes. The potential gap between hydrogen and oxygen evolution reaction (the standard

reduction potential E^o of HER = 0 V_{NHE} = 3.04 V_{Li}; E^o of OER = 1.23 V_{NHE} = 4.27 V_{Li}; V_{NHE} = V versus normal hydrogen electrode) does not exceed 1.5 V even when considering their kinetic overpotentials.[10] Therefore, both HER and OER should be carefully considered when the symmetric $LiMn_2O_4$||$LiMn_2O_4$ cell is charged.

The reduction potential of HER and OER is tunable by pH. At pH 0 (the pH of the standard state), the reduction potential of $LiMn_2O_4/Li_2Mn_2O_4$ (2.9 V_{Li}) is more negative than that of HER (< 3.04 V_{Li}). Hydrogen would be generated on anode during charge from the thermodynamic standpoint. Fortunately, the HER is kinetically unfavorable due to its sluggish kinetics. That is to say, such a small overpotential generate an insignificant HER current. However, the proton co-insertion problem encourages irreversibility leading to poor cyclability in acidic environments. [11, 4, 12] even if the electrolyte electrolysis issue is not very serious at pH 0. When pH is increased to avoid the proton co-insertion, the OER could be problematic. At pH 14, for example, the reduction potential of H^+/H_2 (HER) shifts to the value (< -0.84 V_{NHE} or 2.20 V_{Li}) more negative than that of $LiMn_2O_4/Li_2Mn_2O_4$ (2.9 V_{Li}) so that the HER does not need to be considered. On the other hand, oxygen is generated on cathode during charge because the reduction potential of $Mn_2O_4/LiMn_2O_4$ (> 3.9 V_{Li}) is more positive than that of O_2/H_2O (OER at > 3.43 V_{Li}). Therefore, a delicate pH control is required to proceed both $LiMn_2O_4/Li_2Mn_2O_4$ and $Mn_2O_4/LiMn_2O_4$ electrochemistry within the electrochemically stable potential window of the aqueous electrolyte.

In this work, the failure mechanisms of electrode and electrolyte were detoured by adopting a nano-engineered active material and a super-concentrated aqueous electrolyte. The a-few-layer-graphene-wrapped $LiMn_2O_4$ (LMO@Gn) was used as the active materials of both electrodes. It was reported in our previous work that the LMO@Gn showed significantly improved reversibility of the 3 V reaction (equation 2) leading to prolonged cyclability. The use of high concentration lithium salt in water (therefore, water-in-salt electrolyte or WiSE) extended the electrochemical stability of water by trapping all water molecules by cations and anions. In addition, the aluminum current collectors, which cannot be used in acidic electrolytes due to the corrosion problem, was allowed to be used in the WiSE.[13] With LMO@Gn and WiSE, resultantly, we demonstrated the successful operation of the symmetric LMO@Gn||LMO@Gn cell showing improved coulombic efficiency and cyclability. The cell was much superior to a Ni-MH cell in low temperatures and high rate operation due to the low crystallinity temperature (T_c = -40 °C) and high lithium cation transference number (t_{Li+} = ~0.7) of the WiSE.[10]

1.2 History of battery

The first battery to be estimated is the Baghdad battery, which was built over 2000 years ago and was excavated in 1936. It is thought to have been used for plating, with a structure in which an iron core is placed in the center of a cylindrical earthenware covered with a copper sheet. Since then, however, the knowledge of batteries has been lost, and again in the 18th century, batteries were brought to civilization by Alessandro Volta and Luigi Galvani. [14]

Galvani observed the frog's hind legs spring up when they were in contact with two metals, iron and zinc. He thought that electricity was generated in the animal's body. (Animal electricity) Volta, meanwhile, created a Voltaic pile, a stack of unit cells with brine-soaked cloth between copper and zinc. This enabled high voltage electricity. In both cases, the different metals became the positive and negative electrodes, respectively, and the charge transfer media became the hind legs of the frog in the case of Galvani and brine in the case of Volta. Volta batteries use copper and zinc as positive and negative electrodes, respectively. There are no copper ions in the electrolyte, so that hydrogen evolution occurs at the positive electrode and zinc oxide at the negative electrode.

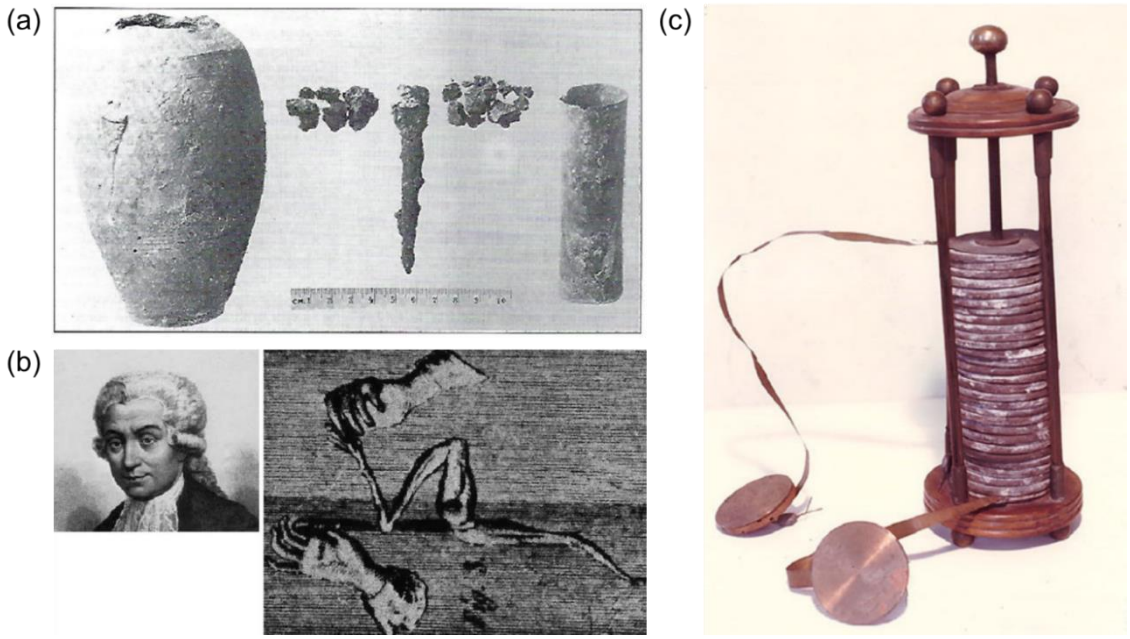

Figure 1 Early battery systems, **(a)** Bagdhad battery which was excavated in 1936 **(b)** Luigi Galvani and his experiment about “animal electricity” on hind legs of a frog **(c)** Voltaic pile invented by Alessandro Volta[14]

Cathode half reaction : $2H^{+}(aq) \rightarrow H_2(g)$ $E^{o} = 0V$ (vs.NHE) (1)

Anode half reaction : $Zn \rightarrow Zn^{2+}(aq) + 2e^{-}$ $E^{o} = -0.76$ V (vs.NHE) (2)

At this time, polarization occurred due to hydrogen bubbles on copper electrodes. In addition, the Voltaic pile, which has problems such as short circuit caused by electrolyte leakage and weak mechanical strength of the cloth soaked with brine, was difficult to operate stably.

These shortcomings were greatly improved in the Daniell cell, which was invented by Daniell in England in 1836. In Daniell's own design, different types of electrolytes were used for the positive and negative electrodes, which were then divided into porous earthen ware. Porous earthenware was placed between the central zinc rod and the copper-covered vessel. The copper sulfate was used for

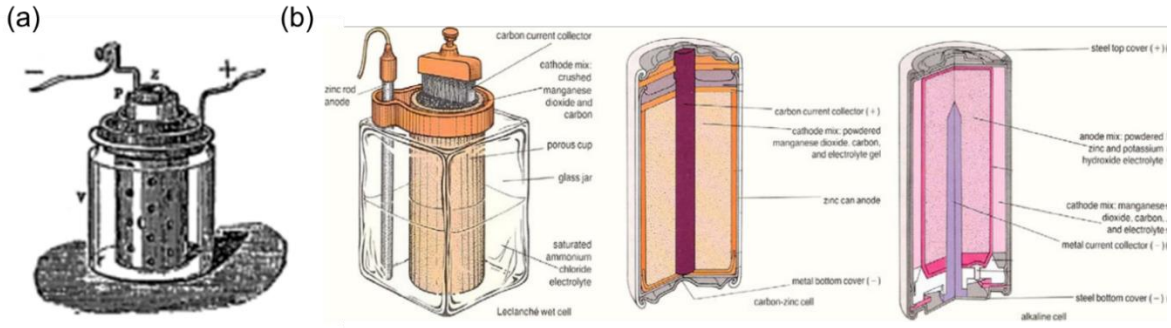

Figure 2 (a) Daniell cell **(b)** Leclanché cell and modern alkarine cell, carbon-zinc cell. Leclanché cell was a wet cell and the other cells are dry cell developed by Carl Gassner[14]

cathodic electrolyte so that copper reduction occurred at the cathode unlike voltaic pile. (equation1) The zinc rod, a negative electrode, was soaked with sulfuric acid to cause zinc oxidation. (equation2)

Cathode half reaction : $Cu^{2+} \rightarrow Cu\ (s)\ \ E^{o} = 0.34V$ (vs.NHE) (1)

Anode half reaction : $Zn \rightarrow Zn^{2+}(aq) + 2e^{-}\ \ E^{o} = -0.76\ V$ (vs.NHE) (2)

The ions pass through the porous pot and porous pot also prevents the solution from mixing, resulting in the electrical neutrality of both aqueous solutions. The Daniell cell became the first battery to be reliably available, and the gravity cell modified from Daniell cell became widely used in electric telegraph network systems in the United States and the UK until the 1950s. In the gravity cell, the porous partition was removed, and the positions of electrodes were fixed that copper on bottom and zinc on top. Copper sulfate crystals were spilled on the cathode surface and filled with distilled water, then driven. The zinc sulfate solution layer formed by dissolved zinc anode was separated from the copper sulfate solution layer due to the density difference and the polarization of the battery. Removing porous walls and the solution separation in this way had the advantage that the internal resistance was greatly reduced. But for the solution to be separated, the battery had to be used statically and kept operating.

The battery, developed by Leclanché in France in 1866, established the structure of cylindrical batteries that are still widely used today. The zinc rod anode was located at the center, and the cathode, which was a mixture of manganese oxide active material and carbon to increase conductivity, was dispersed in an ammonium chloride solution. Based on this, the dry cell was invented by Carl Gassner in 1886. In dry cell, ammonium chloride salt and plaster were mixed instead of aqueous ammonium chloride solution. A minimum amount of water was added to enable ion transport and prevent the

electrolyte leakage and polarization. As a result, unlike previous wet cells, dry cells can be driven reliably, require no maintenance, and have no restrictions on portable. On the other hand, the cathode and anode of Gassner cell are the same as the conventional Leclanché cell. So, the electromotive forces of both batteries are same, 1.5 V. [14]

In 1859, Gaston Plante developed the lead acid battery, which was the first rechargeable battery available to the public. Lead-acid batteries using concentrated sulfuric acid as electrolytes had an electromotive force of 2.1 V, which was higher than that of other batteries. At the positive electrode, hydrogen ions in the acidic electrolyte react with the lead dioxide to generate water. Lead dioxide becomes lead ions by losing oxide, and with sulfate anion it became lead sulfate consequently. It

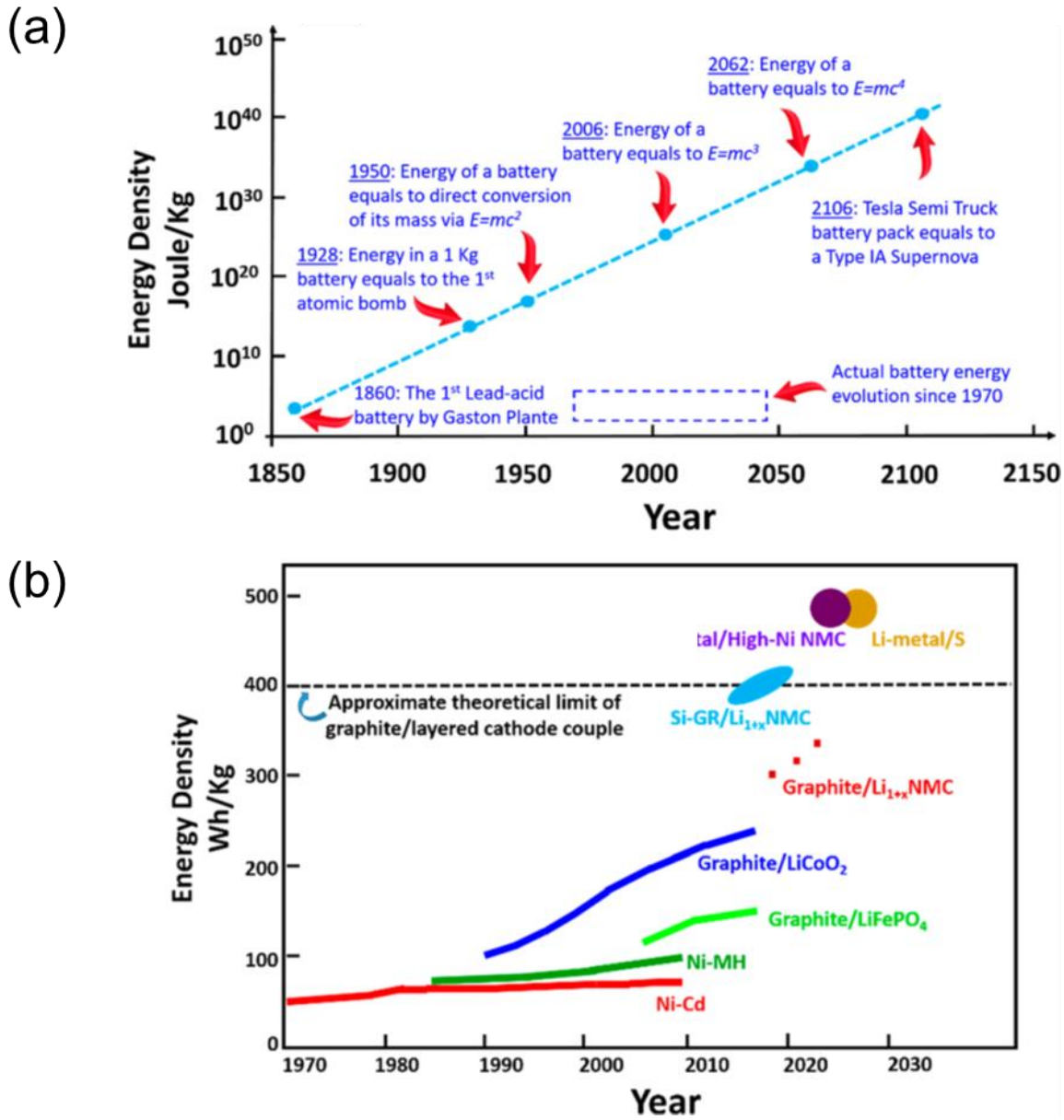

Figure 3 Evolution of energy density of batteries comparing with Moore's law **(a)** predicted evolution when battery developments correspond with Moore's law **(b)** The historical evolution of battery and realistic prediction based on communications between Kang Xu and Dr .Christopher McCoy[15]

adheres to the anode surface. In the anode, lead is converted into lead ions and combined with a negative sulfuric acid solution in the solution to form lead sulfide on the surface of the anode. Later, structurally improved lead-acid batteries, which prevented leakage of sulfuric acid, are still used as automotive batteries in nowadays.

In Sweden in 1901, Waldmar Jugner developed nickel-cadmium batteries, and in the same year Edison developed the Edison cell, nickel-iron battery system. These rechargeable batteries using alkaline hydroxide potassium hydroxide have a low electromotive force, but they are still in use today because they have a long life and low resistance enables generate large currents. Nickel metal hydride batteries developed in 1980s solved the problem of heavy metal contamination in Nickel cadmium or lead acid batteries and had tripled its capacity. Memory effects were also fixed. As such, aqueous electrolyte batteries have expanded their field of battery use through structural and system improvements and have succeeded in lowering their internal resistance.

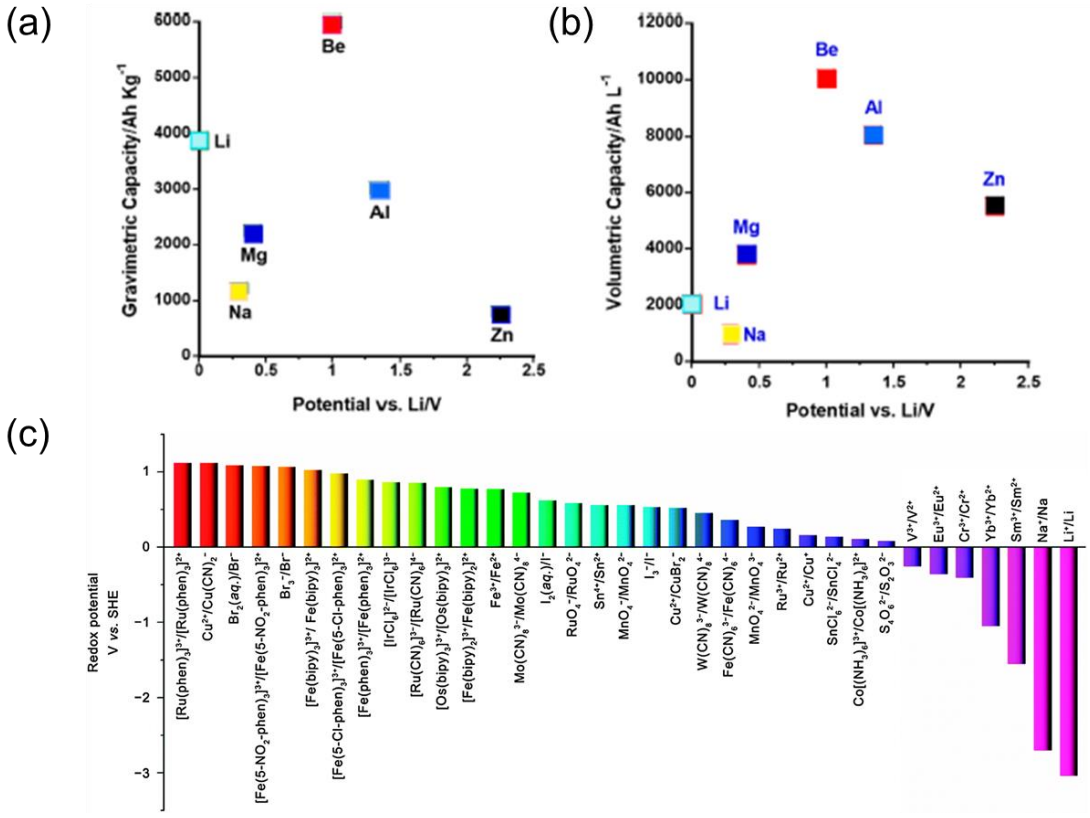

Figure 4 The reasons of high energy density of lithium ion batteries. **(a)** Gravimetric capacities of various metal anodes **(b)** Volumetric capacities of various metal anodes[15] **(c)** Reduction potentials of various metal ions[16]

However, in terms of energy density, the development of the battery was slow. Compared with Moore's Law, which observed by Moore that doubles the performance of semiconductor integrated circuits every two years, the battery's energy density remained in place from 1800 to the early 1900s.

Improving the energy density of a battery is difficult because it overcomes the limitations of all three factors, positive and negative materials and electrolytes. To increase the energy density, the capacity and the operating voltage must be increased, and to increase the operating voltage, the reduction potential difference between the positive and negative electrodes must be maximized. In addition, there must be no side reaction such as solvent decomposition in the electrolyte during cell driving, and thus, stable driving should be possible.[15]

In the late 1900's, the use of electrical energy has expanded into a wider field and demand has increased, and attempts have been made to utilize lithium ions. Lithium has a much higher theoretical capacity of 3860 Ah kg^{-1} than zinc's theoretical capacity of 820 Ah kg^{-1}. In addition, the reduction potential is very low compared to other ions has a great advantage in improving the energy density. Early lithium-ion batteries used lithium metal as a negative electrode and used a carbonate-based organic electrolyte with a wide voltage window due to the low reduction potential of lithium.[16]

The stability and cyclability of the early lithium batteries were very poor due to the dendrite formation at the lithium metal anode and the high reactivity of that. The problem of incomplete suppression of dendrite was a problem for commercialization. As a result, it was possible to secure

stability by intercalation with graphite rather than directly depositing lithium ions with lithium metal. This type of battery has been used in 1990 in developing a battery using lithium cobalt oxide as an anode in Sony. The high energy density batteries have made cell phones lighter and contributes to the spread of electric energy use such as EVs.[15]

1.3 Aqueous electrolytes in Li ion batteries

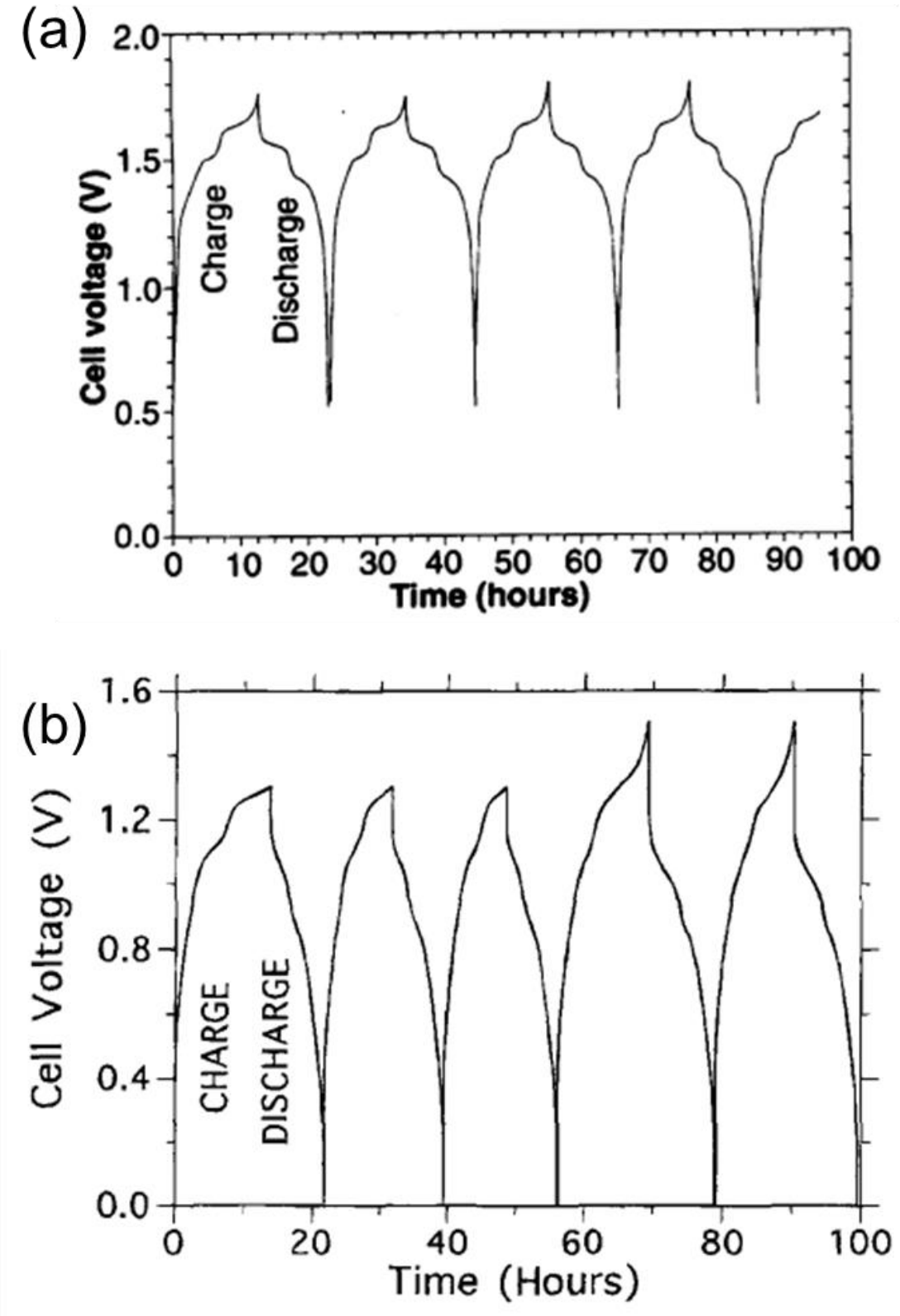

Figure 5 The voltage profiles versus time of **(a)** $LiMn_2O_4/VO_2$ cell[17] and **(b)** $LiMn_2O_4$/ γ-$Li_{0.36}MnO_2$[7]. The applied currents were ±1 mA at 30ºC

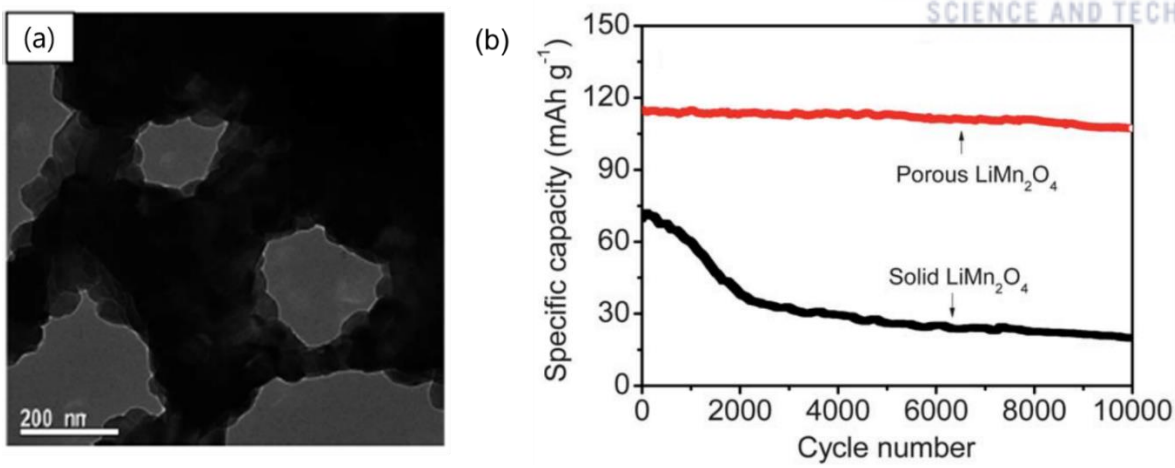

Figure 6 (a) The image gained by transmission electron micrographs (TEM) of the synthesized porous $LiMn_2O_4$. **(b)** Specific capacity plot of porous $LiMn_2O_4$ and solid $LiMn_2O_4$ at current density of 1000 mA g^{-1}. [18]

The organic electrolytes used in current battery systems guarantee high energy density and lifespan with wide voltage window and stability, but at the same time have disadvantages such as low ion conductivity (~ 10 mS cm^{-1}), environmental pollution and explosion due to flammability. Among the problems of organic electrolytes, the explosion problem is fatal for being used as a battery for electric vehicles. Aqueous electrolytes are free from that due to the high heat capacity of water. In addition, it has eco-friendly feasibility and high ion conductivity (˜150 mS cm^{-1}), which is advantageous for rapid charging and discharging which is recently required virtue. However, low electrochemical stability due to water decomposition limits the use of aqueous electrolytes. The low coulombic efficiency and poor cyclability of water-based lithium ion batteries are also due to water decomposition.[4]

In 1994, Dahn first applied an aqueous electrolyte to a lithium ion battery.[17] His first aqueous rechargeable lithium ion battery (ARLB) used $LiMn_2O_4$ (LMO) as the positive electrode, VO_2 as the negative electrode and 5 M $LiNO_3$ with 0.001 M LiOH aqueous solution as the electrolyte. During charging and discharging, the $LiMn_2O_4 \leftrightarrow Mn_2O_4$ reaction occurs at 4.2 V_{Li} on the positive electrode and the $VO_2 + xLi^+ + xe^- \leftrightarrow Li_xVO_2$ reaction occurs at about 2.7 V_{Li} on the positive electrode. This resulted in a battery with an electromotive force of 1.5 V. In 1995, Dahn's next study tested a wider variety of anode materials and electrolytes.[7] $LiMn_2O_4$, $Li_{0.36}Mn_2O_4$, and VO_2 were used as anodes. LMO anode used for $LiMn_2O_4 \leftrightarrow Li_2Mn_2O_4$ reactions occurring at $3V_{Li}$. 5 M $LiNO_3$, 5.7M $LiNO_3$, 10 M LiCl, 1.5 M Li_2SO_4, 8 M Lithium acetate aqueous solutions were used as the electrolyte. However, the anodes using the LMO 3 V region reaction did not operate stably due to the instability described in 1-4 section, and other types of cells also showed a drastic capacity fade due to water decomposition after 20 cycles.

Since then, various attempts have been made to improve water-based batteries. One of them was the improvement of electrode materials. In 2011, Yuping Wu et al. synthesized porous LMO

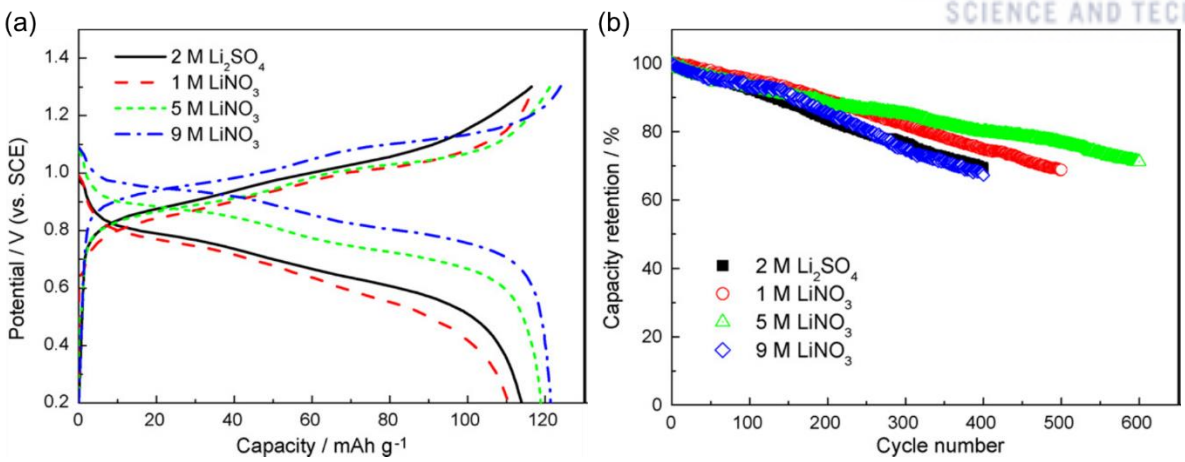

Figure 7 (a) Voltage profiles and **(b)** cycle test plots of $LiMn_2O_4$/activated carbon cells in various densities of $LiNO_3$ aqueous electrolyte. Applied current densities were 500 mA g^{-1}.[19]

cathode to improve their life characteristics and rate capability. [18]Porous LMO was synthesized by infiltrating the solution for LMO synthesis into the polystyrene template and heat-treating it. In this study, only adsorption of ions is used, not electrochemical reactions by using activated carbon as anode. It has a large capacity, can be thought as a half cell. On the average, it showed an electromotive force of 1.0 V and maximized the output by using 0.5 M Li_2SO_4 aqueous solution as electrolyte. Porous LMO showed higher capacity, better cyclability and rate capability than conventional LMO. Porous LMO was stable at up to 10,000 cycles at 1000 mA g^{-1} with specific capacity of ~110 mAh g^{-1}

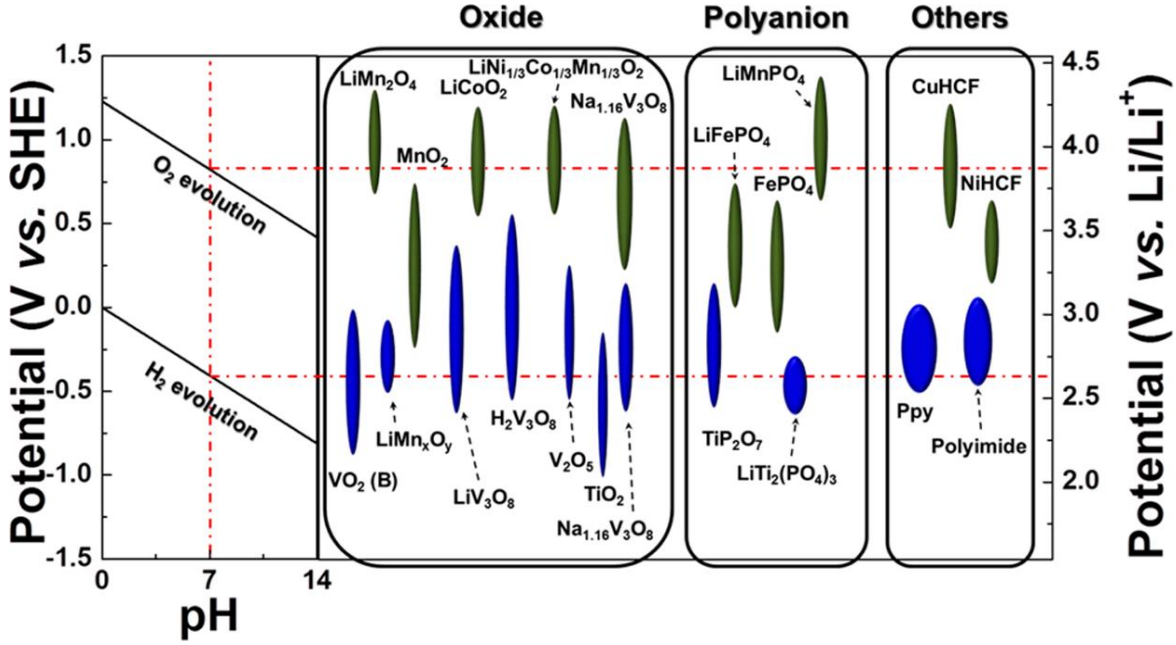

Figure 8 Electrodes used in traditional dilute aqueous electrolyte which of reduction potential must be inner of narrow voltage window of aqueous electrolytes. The reaction potentials of oxygen evolution reaction and hydrogen evolution reaction are affected by pH. The relation between potential and pH follows Nernst equation.[4]

There were also studies about electrolytes. In 2009, Anbao Yuan tested electrochemical performance by experimenting with various concentrations of $LiNO_3$ solutions (1, 2, 5, 9 M). LMO and activated carbon was used as anode and cathode respectively, and 5 M $LiNO_3$ aqueous solution was shown to be the best by comparing cyclability and rate capability.[19]

According to the Nernst equation (1), the lower the pH, the higher the OER potential and the lower the HER potential. It was attempted to suppress OER at the positive electrode or HER at the negative electrode, but failed due to proton co-insertion in acidic environment, active material damage and dissolution in extreme base or acidic environment. In order to use the neutral aqueous solution was forced.[4]

Nernst equation:

$$E = E^0 - \frac{RT}{nF} ln \frac{[Red]}{[Ox\}}$$

These studies tried to increase the coulombic efficiency and cyclability of ARLB, but because they did not solve the fundamental water decomposition, sacrifice of energy density was inevitable. For stable battery operation, only the reaction in the narrow voltage window of the aqueous solution is available, thereby limiting the electrode material selection.

This lack of progress in water-based battery systems was brought to a new stage in 2015 by the discovery of high-density electrolytes in Kang Xu Group. [10]In previous that work, bis(trifluoromethane sulfonyl) imide (TFSI) anion mainly used in ionic liquids. It has low charge density due to huge anion and weak interaction between cation and anion. As a result, LiTFSI salt showed much higher solubility than conventional salts. Kang Xu et al. have developed a water-in-salt electrolyte (WiSE), a 21-m LiTFSI aqueous solution with an overwhelming amount of solute compared to solvents.

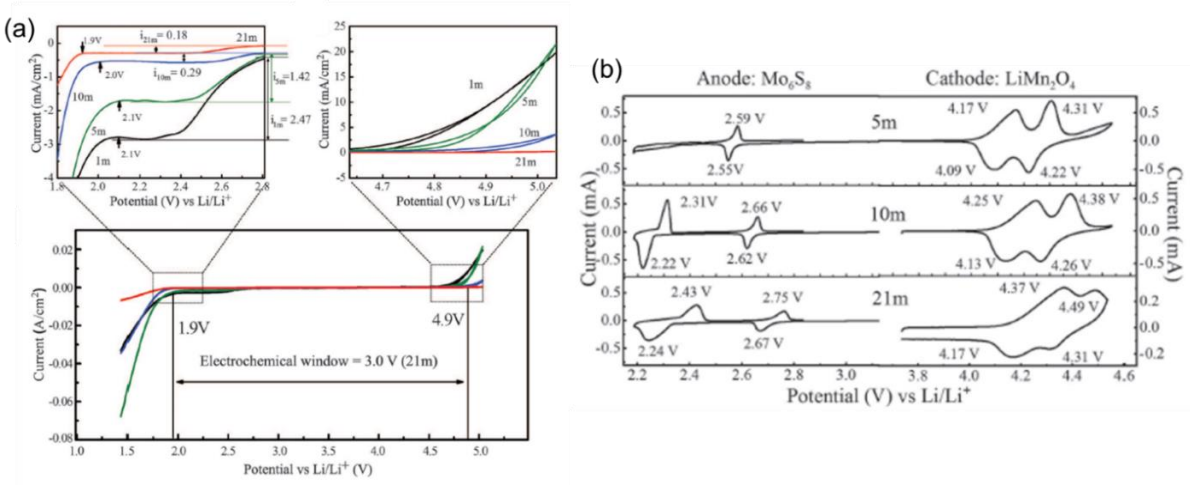

Figure 9 (a) Voltage window of various concentration LiTFSI aqueous electrolyte revealed by cyclic voltammetry using stainless steel as working electrode and platinum foil as counter electrode, Ag/AgCl as reference electrode. Scan rate was 10 mV s^{-1}. **(b)** Cyclic voltammetry using Mo_6S_8 anode and LMO cathode in various concentration LiTFSI aqueous electrolyte[10]

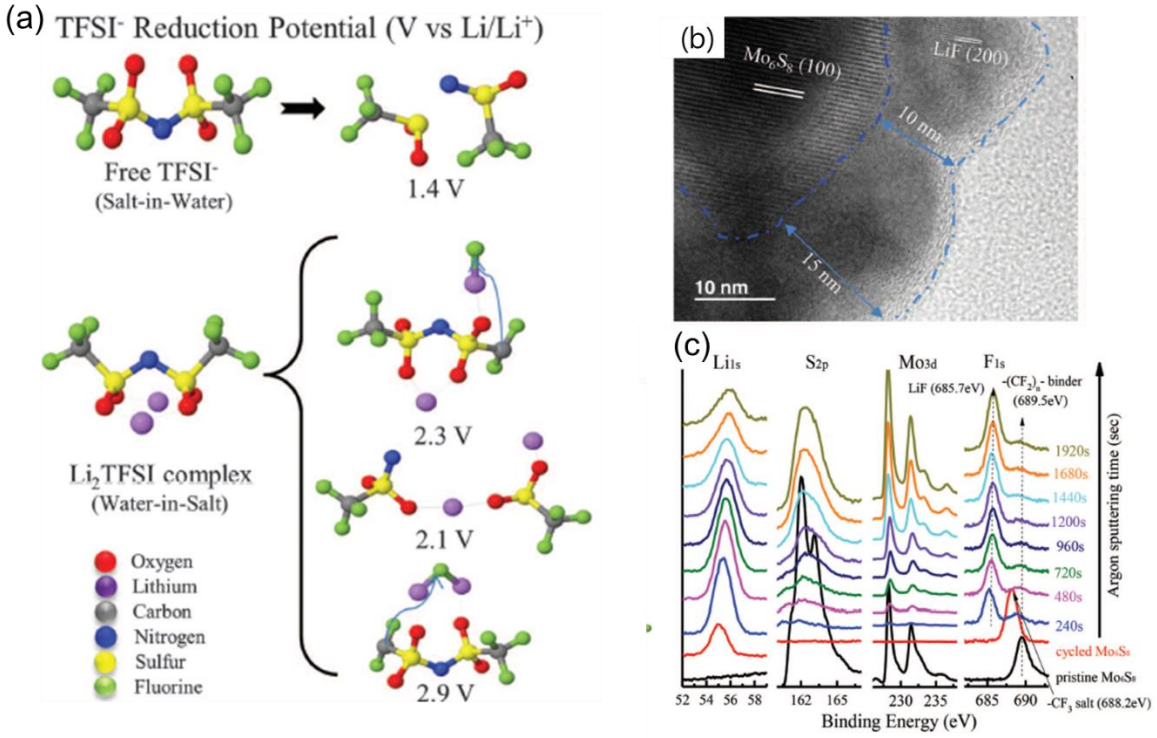

Figure 10 (a) Reduction potentials of TFSI anion in dilute electrolyte and WiSE. G4MP2 quantum chemistry calculations was used for calculating. **(b)** TEM images of Mo_6S_8 formed SEI layer after cycling **(c)** XPS spectrum of pristine Mo_6S_8 and cycled Mo_6S_8 in WiSE. [10]

The activity of water molecules in WiSE becomes very low. This is primarily due to the low concentration of water in the solution due to excess salt. In addition, since the anion that is not solvated in the existing dilute aqueous solution participates in the solvation shell, the concentration of anions on the electrode surface is higher than in the dilute aqueous solution, and thus water molecules are excluded from surface of anode.

The solvated TFSI anions forms complex in WiSE and the reduction potential of TFSI anion increases from former 1.4 V_{Li} to 2.9 V_{Li}. Since the hydrogen evolution reaction occurs at approximately 2.6V_{Li} at neutral pH, the SEI layer is formed by TFSI anion reduction before water is decomposed at the anode. X-ray photoelectron spectroscopy and TEM confirmed that the LiF based SEI layer was formed in WiSE.

Due to reduced water activity and SEI layer formation, the voltage window of WiSE was greatly widened. In the cyclic voltammetry using stainless steel as the working electrode and platinum as the counter electrode, the hydrogen evolution reaction occurs at 1.9 V_{Li} and the oxygen evolution reaction occurs at 4.9 V_{Li}, which has a wider 3.0V electrochemical window than the conventional aqueous electrolyte. In this paper, they implemented a battery system with an average electromotive force, 2 V using LMO as the cathode and Mo_6S_8 as the anode. The increased electromotive force allowed the

energy density of 100 Wh kg^{-1} to be significantly improved from the 75 Wh kg^{-1} shown by existing LMO / VO_2 battery systems.

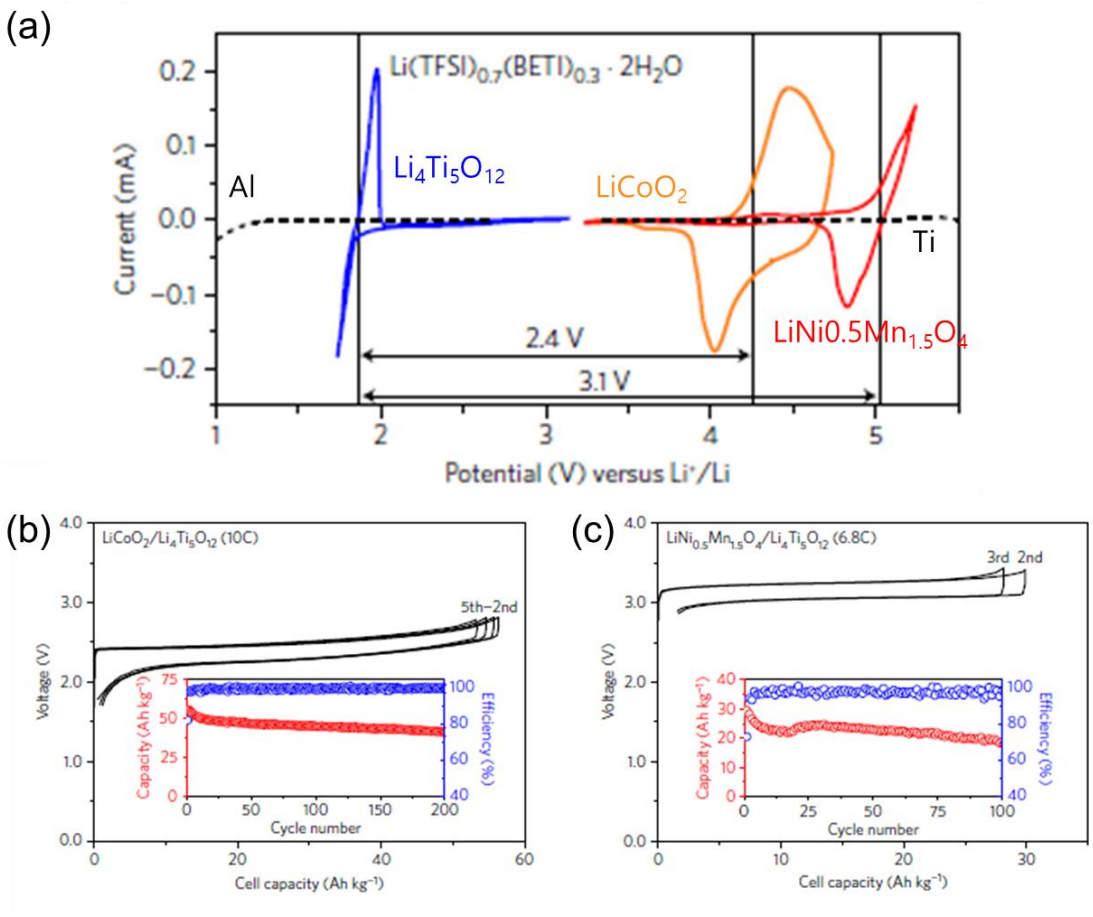

Figure 11 (a) Electrochemical stability of hydrate melt electrolyte revealed by cycle voltammetry using various electrodes as working electrodes. Scan rate was 0.1 mV s^{-1}. **(b), (c)** The voltage profiles and cycle plots of **(b)** $LiCoO_2/Li_4Ti_5O_{12}$ battery system at 10 C and **(c)** $LiNi_{0.5}Mn_{1.5}O_4$/ $Li_4Ti_5O_{12}$ at 6.8 C in hydrate melt electrolyte[20]

Also noteworthy among other WiSE characteristics found in the same paper is thermal stability. As measured by differential scanning calorimetry (DSC), no change of state was observed near the freezing point of water in the 21 m LiTFSI solution and the crystallization temperature was observed at -41.9 °C.

Disadvantages of WiSE include high viscosity and low ionic conductivity. Due to the excess salt in WiSE, the fluidity is only 0.02 cp^{-1} and the ionic conductivity is only about 10 mS cm^{-1}.[10] However, since 0.7 of the transference number(t_{Li}^+) is much higher than that of conventional electrolytes, the actual conductivity is 7 mS cm^{-1}, which is higher than conventional EC / EMC based organic electrolytes (~ 4 mS cm^{-1}).[21]

In 2016, Atsuo Yamada Group developed Hydrate melt electrolyte by adding $LiN(SO_2C_2F_5)_2$ (BETI) salt to an existing 21 m LiTFSI solution.[20] The molar ratio of LiBETI and LiTFSI was set to a molar ratio of 0.7: 0.3: 2 (LiTFSI: LiBETI: H_2O), an eutectic point that minimizes the amount of water. In terms of molar concentration, 21 m LiTFSI, 7 m LiBETI aqueous solution. The water activity in the

hydride melt electrolyte drops to 0.12 and the ionic conductivity is 3 mS cm^{-1}, lower than that of the existing WiSE due to the addition of additional salts. The voltage window of the hydride melt electrolyte becomes wider as the amount of free water molecules decreases and the activity of water decreases. In cyclic voltammetry using stainless steel as the working electrode and platinum as the counter electrode, OER occurred at 5.05 V and HER occurred at 1.25 V_{Li} when the working electrode was used as aluminum. Through this, battery systems using $Li_4Ti_5O_{12}$ cathode (1.7 V_{Li}) on aluminum current collector and $LiNi_{0.5}Mn_{1.5}O_4$ reacting at 5 V_{Li} and $LiCoO_2$ (LCO) reacting at 4.4 V_{Li} were implemented. LNMO and LTO have higher electromotive force thanks to active materials that were not used due to hydrogen and oxygen generation in normal WiSE. The LCO has a higher 50mAh g^{-1} (25 cycles) and the electromotive force is 2.3V. When LNMO is used, the electromotive force is 3 V and the capacity is expressed at 25 mAh g^{-1} (25 cycles). The battery systems realized energy density of over 150 Ah Kg^{-1}.

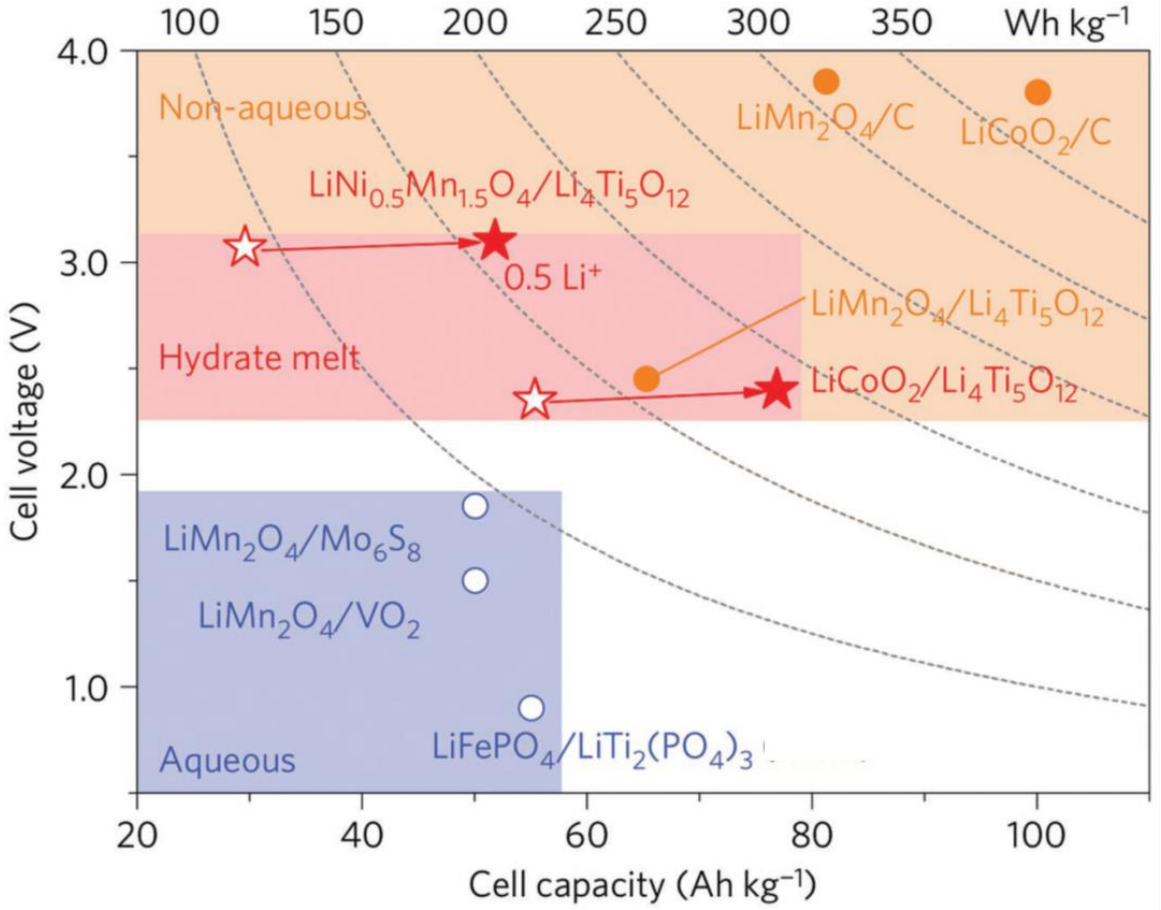

Figure 12 Energy density plot versus capacity of various battery systems in different types of electrolyte. Empty circles and stars mean theoretical energy densities and full circles and stars mean experimental energy density[22]

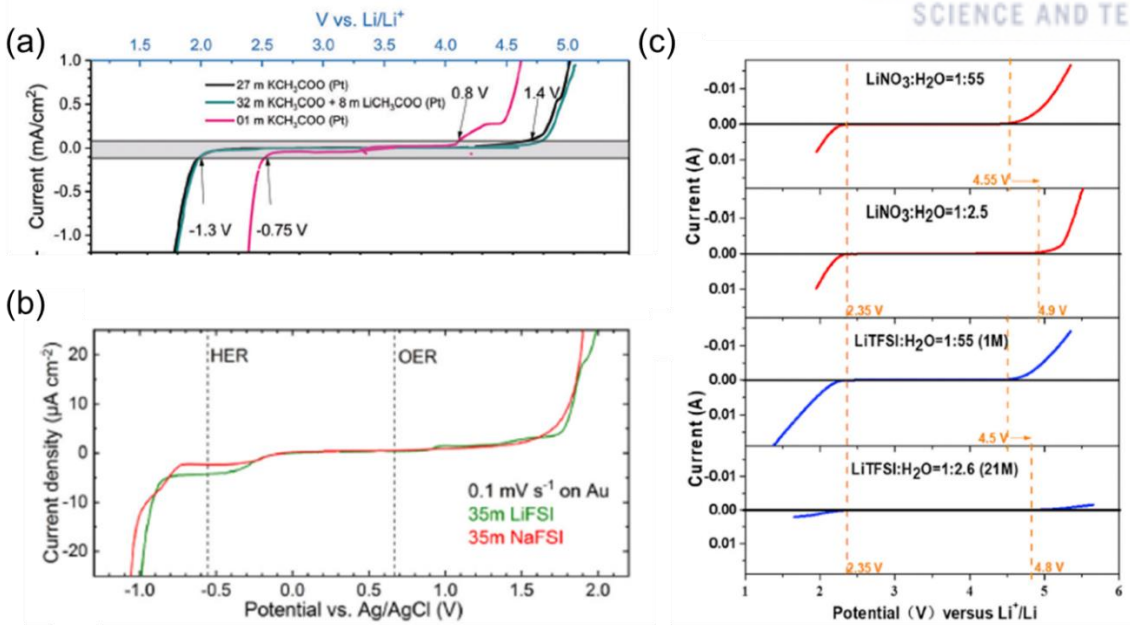

Figure 13 Electrochemical stability of **(a)**mixed cation acetate WiSE[23] and **(b)** FSI based WiSE[24], **(c)** various concentration of $LiNO_3$ aqueous electrolyte[25] revealed by cycle voltammetry.

In addition, there have been attempts to further reduce water activity by adding lithium trifluoromethane sulfonate (LiOTF) salt to the existing WiSE or by adding polymer PEO. Unlike Hydrate melt electrolyte, the voltage window was not widened, but the cyclability and coulombic efficiency were improved, resulting in higher stability. In 2017, Kang Xu et al. added 1,1,2,2-tetrafluoroethyl-20,20,20-trifluoroethyl ether (highly fluorinated ether) as an inhomogeneous additive to WiSE with 10 wt% PEO and 7 m LiOTF.[26] They succeeded in forming the SEI layer and at the same time significantly reduced the activity of water on the electrode surface. Through this, a 4.0 V aqueous battery using graphite and lithium metal as a anode was realized.

On the other hand, there have been studies to make super-concentrated solutions using salts other than LiTFSI. In 2018, Yi Cui Group developed mixed cation acetate WiSE using Lithium acetate and Potassium acetate.[23] Since the electrolyte is difficult to secure high solubility due to the high charge density of Lithium, potassium is used together. It is eco-friendly by not using toxic TFSI anion. This electrolyte, mixed with 32 m KOAc and 8 m LiOAc, inhibited HER up to 1.3 V_{Li} when glassy carbon was used as the working electrode, and OER was not observed even at 5 V_{Li}. They succeeded in making a 2.0 V cell using an LMO / c-TiO2 electrode. When they increased the C rate from 0.5 C to 1 C, the capacity was reduced by more than half, showing poor rate capability.

In the same year, Kang Xu Group found that the ultra-high concentration solution, in which the $LiNO_3$ salt was dissolved until the molar ratio of water was 1: 2.5 ($LiNO_3$: H_2O), had a voltage window of about 2.5 V.[25] When the molar ratio is converted to molar concentration, it becomes approximately 18 m LiNO3 solution, which exceeds the solubility at 25 °C, and the paper says that it was made at 35 °C. In 2019, Kühnel et al. put LiFSI and NaFSI up to 35 m and realized the voltage windows above 2 V. These

solutions did not confirm the formation of the SEI layer, indicating that the voltage window can be widened by reducing the free water molecules and reducing the activity of the water.

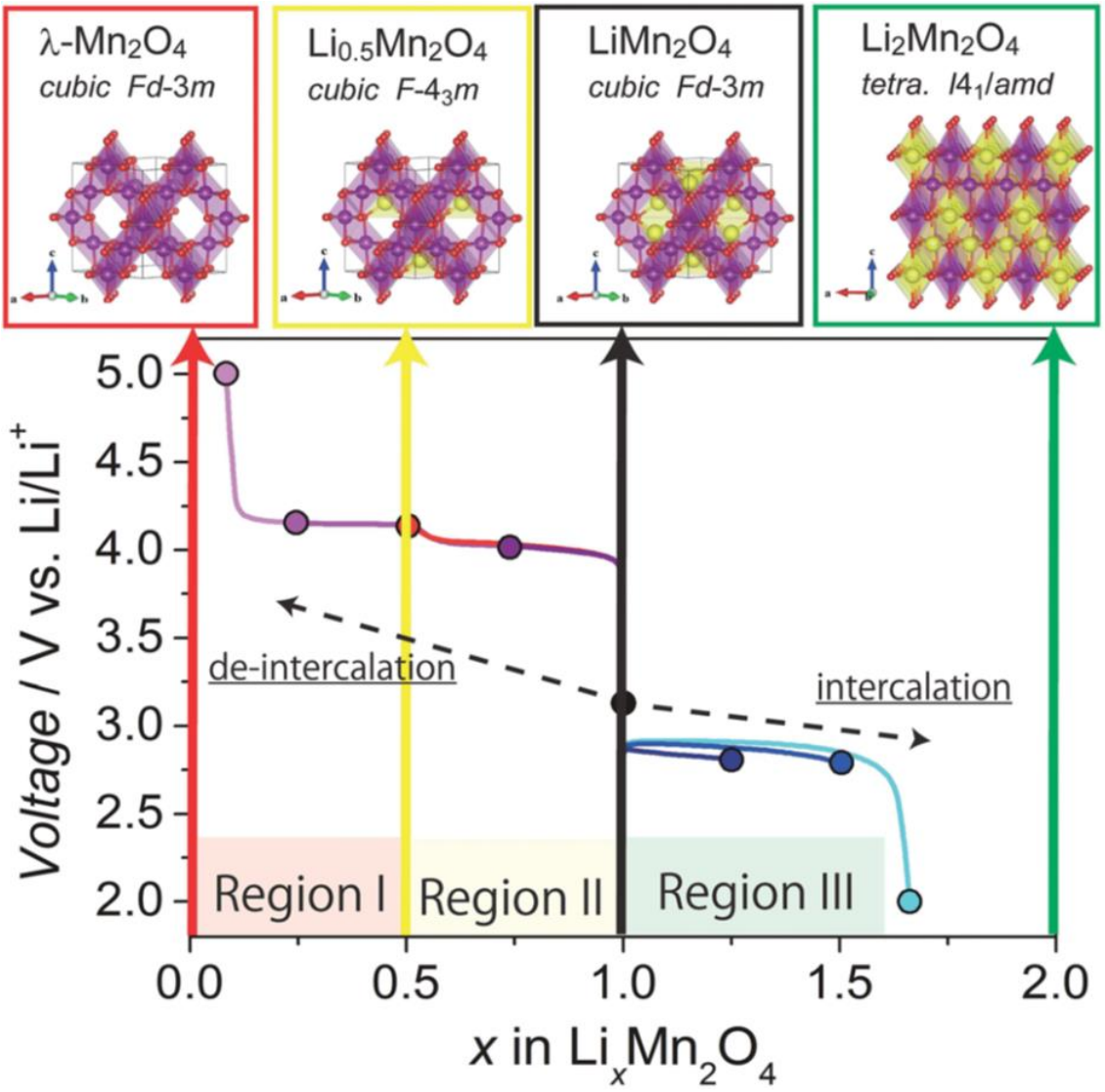

Figure 14 Phase of $Li_xMn_2O_4$ ($0 \leq x \leq 2$) and voltage plot versus amounts of intercalated lithium ion. Purple octahedrons mean MnO_6, red ones are oxide ions and yellow ones are lithium ions.[27]

1.4 Jahn-Teller distortion in lithium manganese oxide

LMO has been attracting attention since its first commercially available cathode material, LCO, due to its low cost and low pollution. LMO, used as the anode in Dahn's first ARLB, causes lithium intercalation to occur in multiple voltage ranges.[7] In λ-Mn_2O_4 with cubic spinel structure, lithium intercalation occurs at 4 V_{Li} and the chemical composition is changed to LiMn2O4. This reaction produces a capacity of 100 mAh g^{-1}.

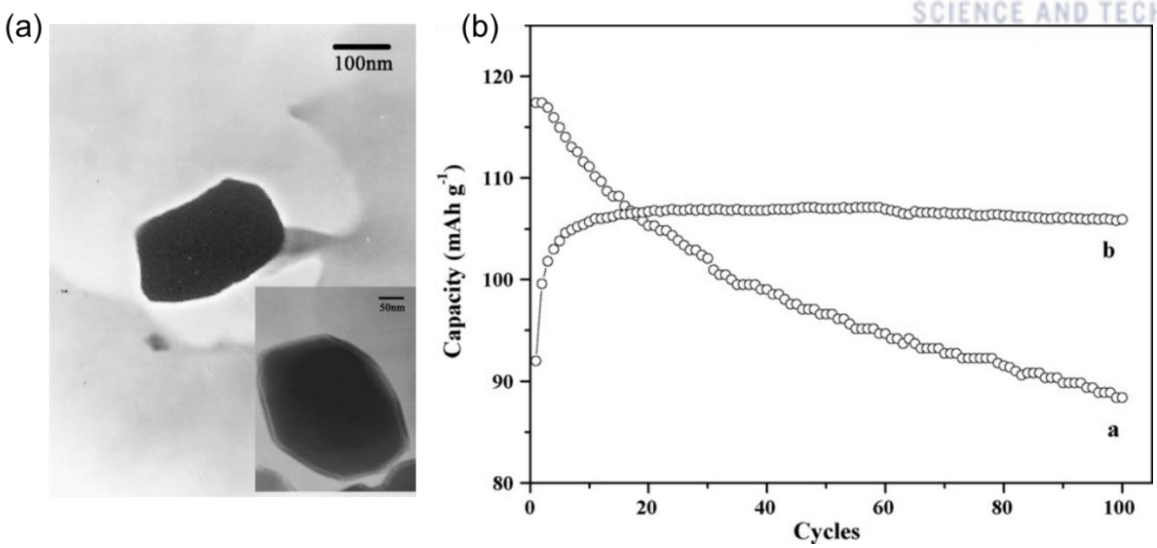

Figure 15 (a) TEM image of conventional LMO and modified LMO formed $LiNi_xMn_{2-x}O_4$ layer **(b)** Cycle test for 4 V region reaction of LMO for pure LMO and modified LMO. The voltage cut offs were 3.5 V and 4.3 V at current density of 0.1 mA cm^{-1}. [28]

The open circuit voltage (OCV) of $LiMn_2O_4$ is 3 V_{Li} and the structure of $LiMn_2O_4$ is determined by the oxidation number composition of Mn. Ideally, Mn ions in $LiMn_2O_4$ are 50% Mn^{3+} and Mn^{4+}, respectively. At this time, $LiMn_2O_4$ had a cubic spinel structure. When the amount of Mn^{3+} exceeds 50 percent, structure of $LiMn_2O_4$ begins to change into tetragonal, resulting in Jahn-Teller distortion. At high C rates, the movement of lithium ions in the solution is faster than the dispersion of lithium ions in the electrodes, resulting in frequent Jahn-Teller distortion. This reduces the lifetime characteristics of using the 4 V reaction.[29]

In $LiMn_2O_4$, again lithium intercalation can be, and the reaction is occurred at 3 V_{Li}. $Li_2Mn_2O_4$ has a tetragonal structure and a theoretical capacity of 100 mAh g^{-1}. However, the change from LiMn2O4, which is a cubic spinel structure, to $Li_2Mn_2O_4$, which has a tetragonal structure, causes Jahn-Teller distortion. As a result, a stable 3V region reaction is not usable in bulk LMO and a severe capacity fade occurs.

Attempts to use 3 V response in battery systems have failed due to Jahn-Teller distortion. In aqueous batteries, the 3 V region reaction of LMO was used as the negative electrode. In 1994 and 1995, Dahn tested a symmetric LMO battery system using LMO as a cathode and an anode in 5M $LiNO_3$ aqueous solution. However, the cell experienced a dramatic decrease in capacity in two cycles. In 1996, Wang Pei et al. applied a 5 M LiNO3 solution with varying pH using LiOH and H_2SO_4 in a symmetric LMO battery system.[11]

To overcome the Jahn-Teller distortion and use the 3 V reaction of LMO, Yang-Kook Sun group synthesized sulfur doped spinel structure $LiAl_{0.24}Mn_{1.76}O_{3.98}S_{0.02}$. Lithium metal foil was used as the cathode and 1 M $LiClO_4$ in EC / PC (1: 1) was used as the electrolyte. This material showed a capacity of 100 mAh g^{-1} in the 4 V region reaction and showed good lifetime characteristics. In the 3 V reaction,

the capacity continued to increase until 35 cycles, with a capacity of 130 mAh g^{-1} at the last 35 cycles. In the data using both 4 V and 3 V reactions as the anodic reaction, a capacity of 230 mAh g^{-1} was expressed, and no capacity decrease was observed up to 25 cycle.

In 2009, another method of suppressing Jahn teller distortion by another synthesis was reported by Chunlei Wang. The modified LMO synthesized by adding $Ni(NO_3)_2$ and $CO(NH_2)_2$ when forming the cathode material slurry forms a $LiNi_xMn_{2-x}O_4$ solid solution shell on the surface and suppresses Jahn teller distortion. This improved the lifetime characteristics of the 4 V reaction and did not examine the 3 V reaction.[29]

As such, methods to reduce the amount of Mn^{3+} that causes Jahn-teller distortion by doping other cations to the LMO and to suppress the volume change by forming a layer on the surface have been attempted to prevent Jahn teller distortion.

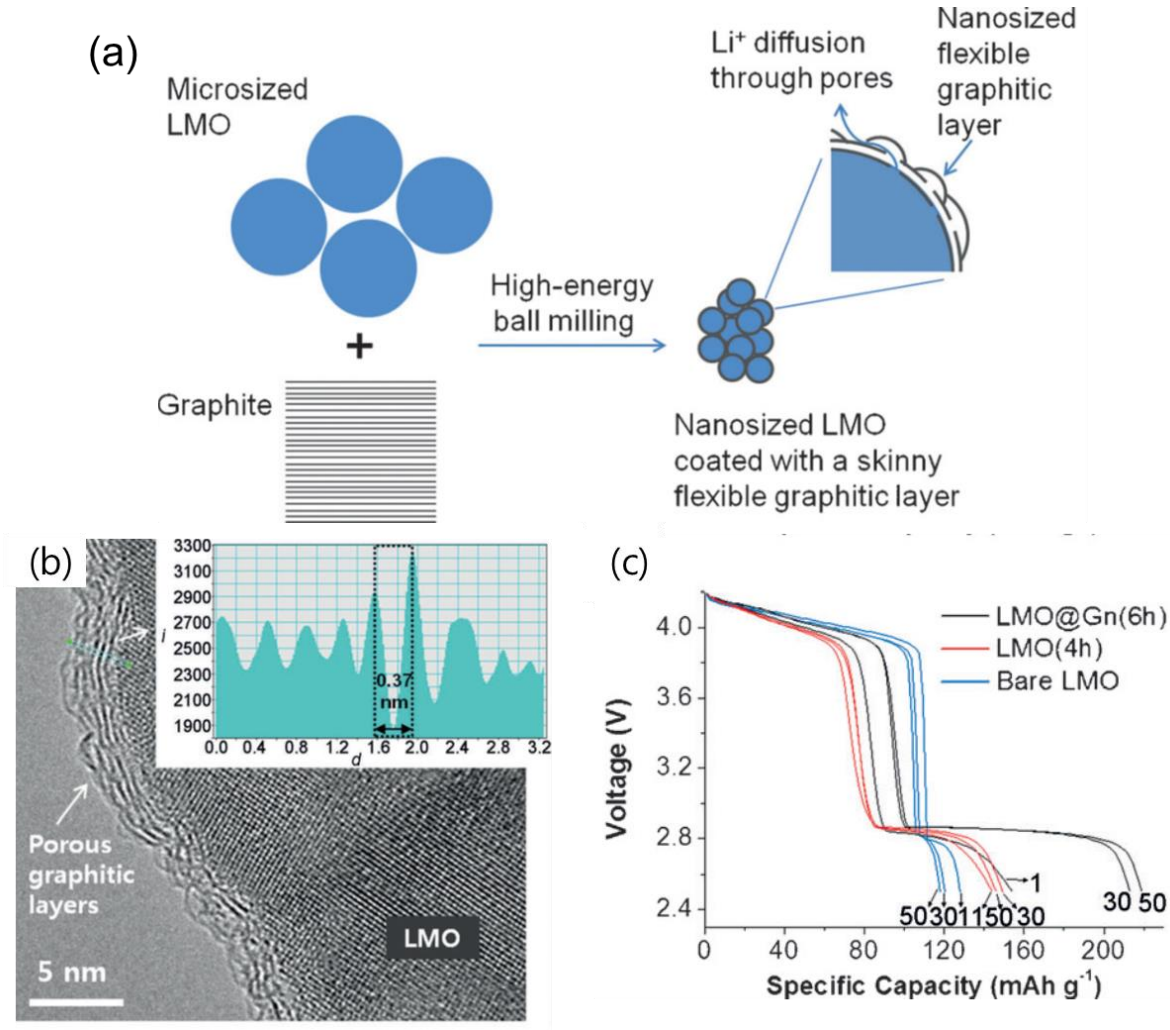

Figure 16 (a) Synthesis of graphite few layer coated LMO(LMO@Gn) by high-energy ball milling **(b)** TEM image of LMO@Gn when the powders ball-milled for 1 hour **(c)** Voltage profiles for two region reactions of various type of LMO cathodes in 0.5 C. (bare LMO and 4 hour ball-milled LMO, LMO@Gn) [9]

In 2014, Noh groups succeeded in suppressing the Jahn-Teller distortion in the simpler way and using the 3 V reaction.[9] Micro-sized LMO and graphite were subjected to high energy ball mill for 6 hours at 80: 7 (LMO : graphite) weight ratio, through which LMO@Gn was coated with thin graphite layer coated on LMO. Graphite layers contributed to the increase in electrochemical performance due to their structural strength and good conductivity. It also prevented the leaching of manganese on the surface, which greatly improved the cyclability. The efficient suppression of Jahn-Teller distortion was demonstrated in cell tests using lithium metal as anode. The capacity of 100 mAh g^{-1} was maintained from 3 V reaction to 60 cycles, and the capacity of 200 mAh g^{-1} was realized when both 4 V and 3 V reactions were used.

2.Experimental

2.1 Preparation of the LMO@Gn electrode

LMO powder (Aldrich, undoped) and graphite (Timcal KS6) were used to synthesize LMO@Gn. The powders are mixed with 80:7 (wt/wt) proportion. The mixed powders were high-energy ball-milled for 6 hours by high energy vibratory ball miller (SPEX 8000D). For 5 g amount of LMO, 6 stainless steel ball which of diameter is 5 mm were used. For preventing oxidation, the mixed powder and balls were carried in argon atmosphere.

Polyvinylidene fluoride (PVDF; Solef 5130) binder and carbon black (Timcal Super P) conducting additive, synthesized LMO@Gn powder were mixed with N-methyl-2-pyrrolidone solvent. The mass ratio of active material, binder, and carbon black was 7: 2: 1 in that order. The slurry was casted on the aluminum foils as current collector for organic electrolyte cells and WiSE cells. Stainless steel 316L foils were used as current collector for aqueous electrolyte cells. When aluminum foil was used as current collector in conventional aqueous electrolytes, severe corrosion reactions were occurred during charging.[13] (**Figure** S2) The mass loading of electrodes was about 1~2 mg cm^{-1}.

2.2 Characterization

Synthesized LMO@Gn powder was identified by X-ray diffraction in **Figure** S1 (XRD; Bruker AXS, D8 advance with Cu-Kα radiation). Pristine and cycled LMO@Gn electrodes were analyzed by X-ray photoelectron spectroscopy (Thermo Fisher K-alpha). Fourier-transformed infrared spectroscopy (FTIR, Varian, Varian 650) was used for revealing strength of O-H bond in aqueous solutions.

2.3 Electrochemical measurement

2032 coin cells were assembled with LMO@Gn as both electrodes (LMO@Gn||LMO@Gn) for cyclability test and rate capability test, impedance measurement. 21 m LITFSI aqueous solution, 1 M $LiPF_5$ in ethylene carbonate/ethyl methyl carbonate (1:2v/v) were used as electrolyte for WiSE SLMO cells and Org SLMO cells, respectively. 5 m and 12 m $LiNO_3$ aqueous solutions are also used as electrolyte for aqueous SLMO cells. Impedances of coin cells were measured by electrochemical impedance spectroscopy using potentiostat (BioLogic VSP-300). Rechargeable nickel metal hydride dry cell (Energizer AAA type) and SLMO coin cells were used in low temperature cell tests.

3.Results

3.1. Concept of symmetric lithium manganese oxide

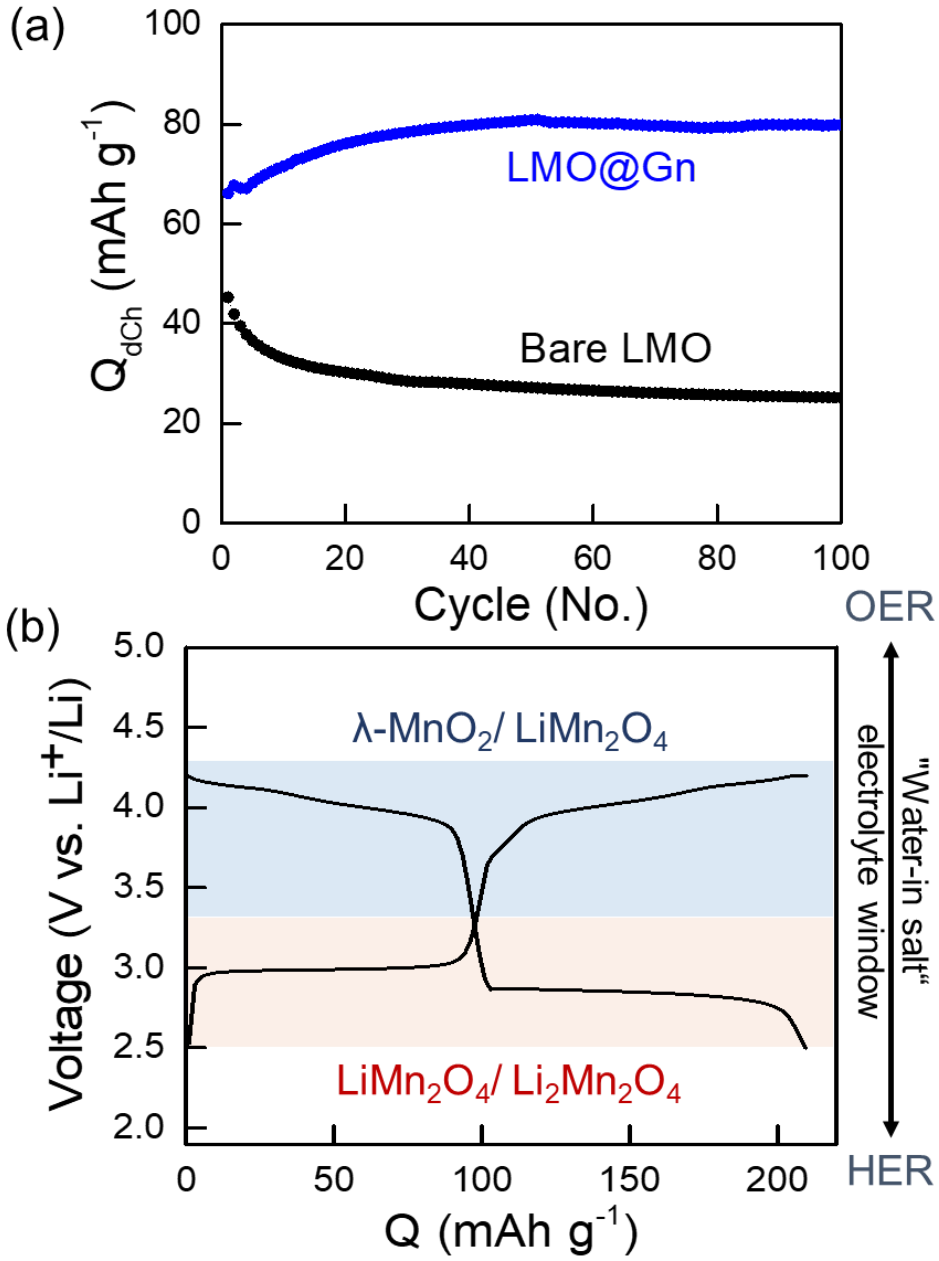

Figure 17 (a) Cyclability test for 3 V region LMO reaction using bare LMO electrode and LMO@Gn electrode in 1 C. **(b)** Galvanostatic charge/discharge potential profile of LMO@Gn || Li metal half-cell in 0.2 C-rate after activation. The yellow region means 3 V region reaction which is second lithium ion intercalation to $LiMn_2O_4$ at charge or deintercalation from $Li_2Mn_2O_4$ at discharge

A few-layer graphene coating on $LiMn_2O_4$ (therefore, LMO@Gn) has been demonstrated to improve the electrochemical reversibility of 3 V reaction.[9] In conventional carbonate-based organic electrolyte (org.), 3 V region reaction of bare LMO and LMO@Gn were tested in **Figure** 17 a. From the half-cell tests when the C rate were 1 C, bare LMO showed poor cyclability and low capacity (45 mAh g^{-1},

maximum capacity during cycle) than LMO@Gn which of capacity (82 mAh g^{-1}, maximum capacity during cycle) and cyclability were great. As reported, graphite coating on micro-sized LMO made 3 V region reaction usable with overcoming Jahn-Teller distortion.

Using both 3 V and 4 V reactions at the same time were also tested in **Figure** 17 b. the discharge capacity showed severely deteriorated even after first cycles when bare LMO||Li half-cell was fully lithiated to 2.5 V ($Li_2Mn_2O_4 \rightarrow LiMn_2O_4$) and then fully delithiated to 4.2 V ($LiMn_2O_4 \rightarrow Mn_2O_4$) in 0.2C. However, LMO@Gn significantly improved the discharge capacities (Q_{dCh} = 209.5 mA h g^{-1} with LMO@Gn) and coulombic efficiency (η_0 = 99.86% with LMO@Gn). Based on LMO@Gn half-cell investigation, we were set the effective cut-off voltages from 0.4 V to 1.65 V for realization of symmetric cells by using LMO@Gn as both cathode and anode.

3.2 Traditional aqueous electrolyte versus "Water-in-Salt" electrolyte

Operation voltage of the rocking chair LMO battery system is about 1 V which is enough low to use water as solvent. Among the various aqueous electrolytes, Lithium nitrate ($LiNO_3$) aqueous solutions are not only the one of the most conventional aqueous electrolytes but also they were tried in Dahn's bare LMO rocking chair battery system. 5 m, 12 m $LiNO_3$ aqueous solution was used as electrolyte with LMO@Gn electrodes in **Figure** 18, 19. The cell using 5 m $LiNO_3$ electrolyte showed very poor initial coulombic efficiency (η_0 = 5.0%) with excessive over-charging (~1200 mAh g^{-1}). At second cycle, the coulombic efficiency was 20 %. The discharge capacity in early stage of cycles (50 mAh/g at first cycle) was also lower than theoretical capacity. (~100 mAh g^{-1}) 12 m $LiNO_3$ aqueous electrolyte showed great capacity (81 mAh/g) in first and second cycle which is close to theoretical capacity and its coulombic efficiency was improved dramatically in first, second cycle. (63, 74%) However, coulombic efficiency during cycle test was remained under 90% until the capacity was decreased severely. The low coulombic efficiency can be one of the suspected points about water decomposition.

Water-based high-concentrated electrolyte (21 m LiTFSI in H_2O; WiSE) showed an improved initial discharge capacity (Q_{dCh}) of 80 mAh g^{-1} and higher initial coulombic efficiency (η_0) of 60% compared to dilute aqueous electrolyte (50 mAh g^{-1} for Q_{dCh} and 5% for η_0) and also organic electrolyte (54 mAh g^{-1} for Q_{dCh} and 73% for η_0). Cyclic voltammograms supported the excellent electrochemical activation from the viewpoint of clearness of redox peaks in the presence of different electrolyte compositions. The clear two cathodic peaks and anodic peaks were obtained continuously in the presence of WiSE while only single and broad peaks were obtained other aqueous and organic electrolytes. (**Figure** S3)

The cell using 5 m LiNO3 in water, dilute aqueous electrolyte showed poor coulombic efficiencies and discharge capacities during the cycles. Also, using 12 m $LiNO_3$ was not successful by severe capacity fade in **Figure** 18, 19. In full cell data, the charge capacity of 1st cycle of dilute aqueous

electrolyte cell was about 1200 mAh g^{-1} when discharge capacity of 1st cycle was only 50 mAh g^{-1}. This irreversible reaction must be OER. In **Figure** 20, the amounts of produced oxygen and

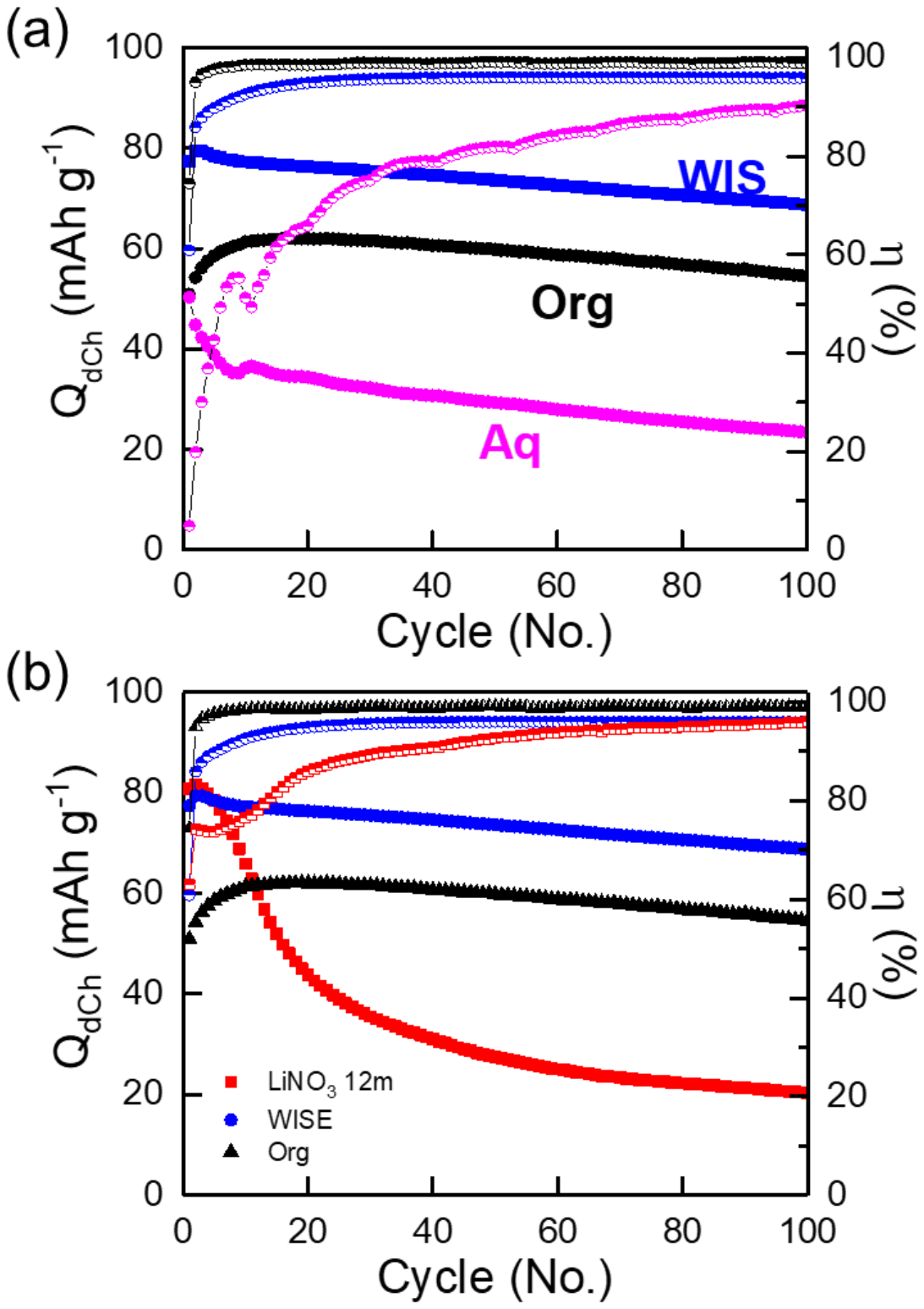

Figure 18 (a) (b) Discharge capacity and coulombic efficiency of graphite coated $LiMn_2O_4$ (LMO@Gn) symmetric cell with various electrolytes at 1 C. (WIS= 21 m LiTFSI aqueous electrolyte, Aq= 5 m $LiNO_3$ aqueous electrolyte, Org= 1 M $LiPF_6$ in EC/EMC (1:2, v/v))

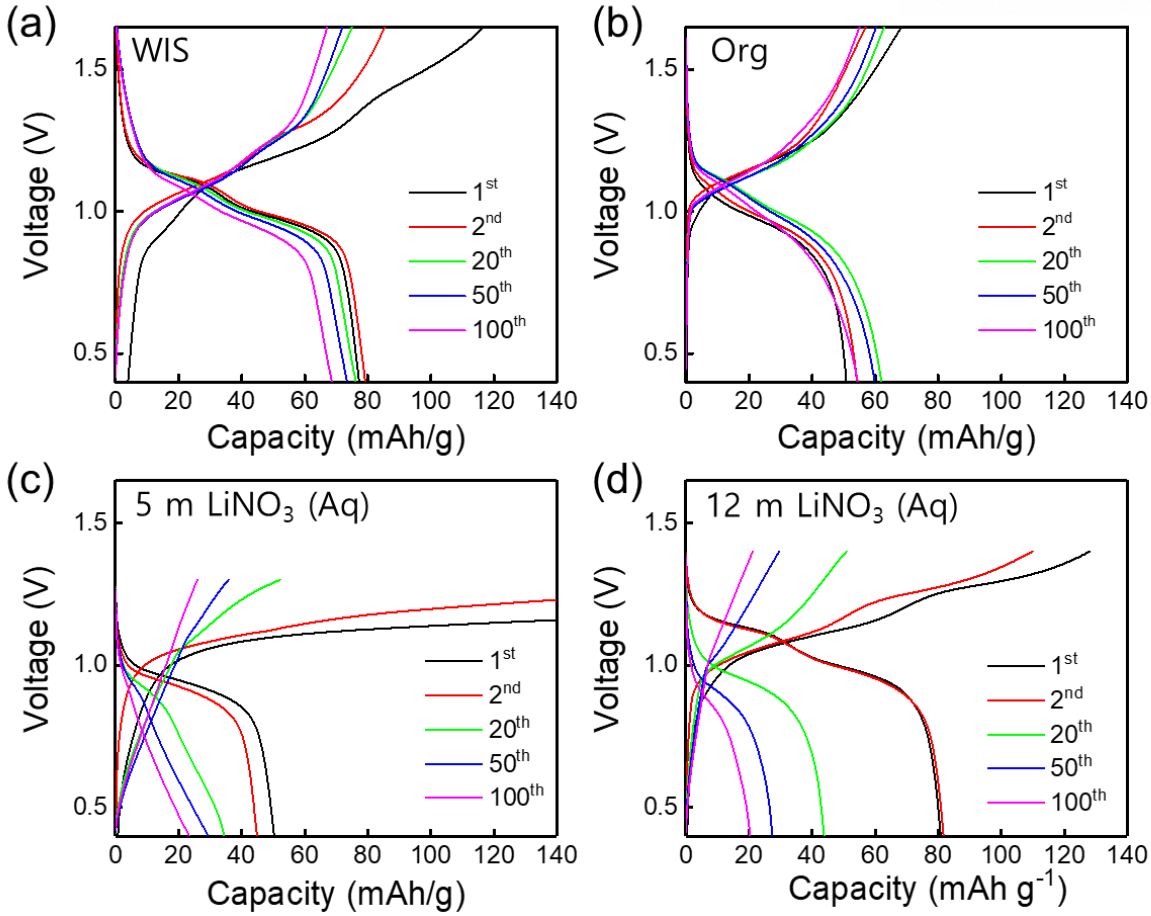

Figure 19 Voltage profiles of SLMO cells at 1 C during 100 cycles using various electrolytes. The cells operated in 0.4 V-1.65 V range for WIS, Org. The cells using $LiNO_3$ aqueous solutions as electrolytes operated in 0.4 V-1.45 V range.

hydrogen in the various aqueous electrolytes during 1st and 2nd cycles of SLMO were figured out by differential electrochemical mass spectrometry (DEMS). When using $LiNO_3$ 5, 12 m aqueous electrolytes, oxygen evolution was identified. In 5 m $LiNO_3$ electrolyte, oxygen gas was produced and the maximum amounts of released oxygen gas per minute was about 260 nmol min^{-1}. In 12 m $LiNO_3$ aqueous electrolyte, the amount of released oxygen gas was smaller than 5 m $LiNO_3$. The average amount of evolved oxygen per minute was about 75 nmol min^{-1}. In WiSE, the amount of released oxygen gas was the least among them. The average amount of released oxygen gas was about 20 nmol min^{-1}. From that, the reason for low coulombic efficiency and instable operating aqueous SLMO was confirmed to be water decomposition, oxygen evolution reaction. In contrast to oxygen gas, hydrogen gas was not detected at all in the samples. Hydrogen evolution reaction (HER)of pure water is occurred at 3 V_{Li} and anode reaction of SLMO battery is also occurred at 3 V_{Li}. However, because of the neutral pH of used electrolytes, HER is occurred at ~2.7 V_{Li}.

Controlling pH could be a solution for overcoming failures of NO_3 based electrolyte. pH of 5 m, 12 m $LiNO_3$ in water are both 6.5 and then the potentials of HER (3 V_{Li} at pH 0) and OER (4.23 V_{Li} at pH 0) are moved to lower side by following Nernst equation. (**Figure** 21) In the condition, HER of

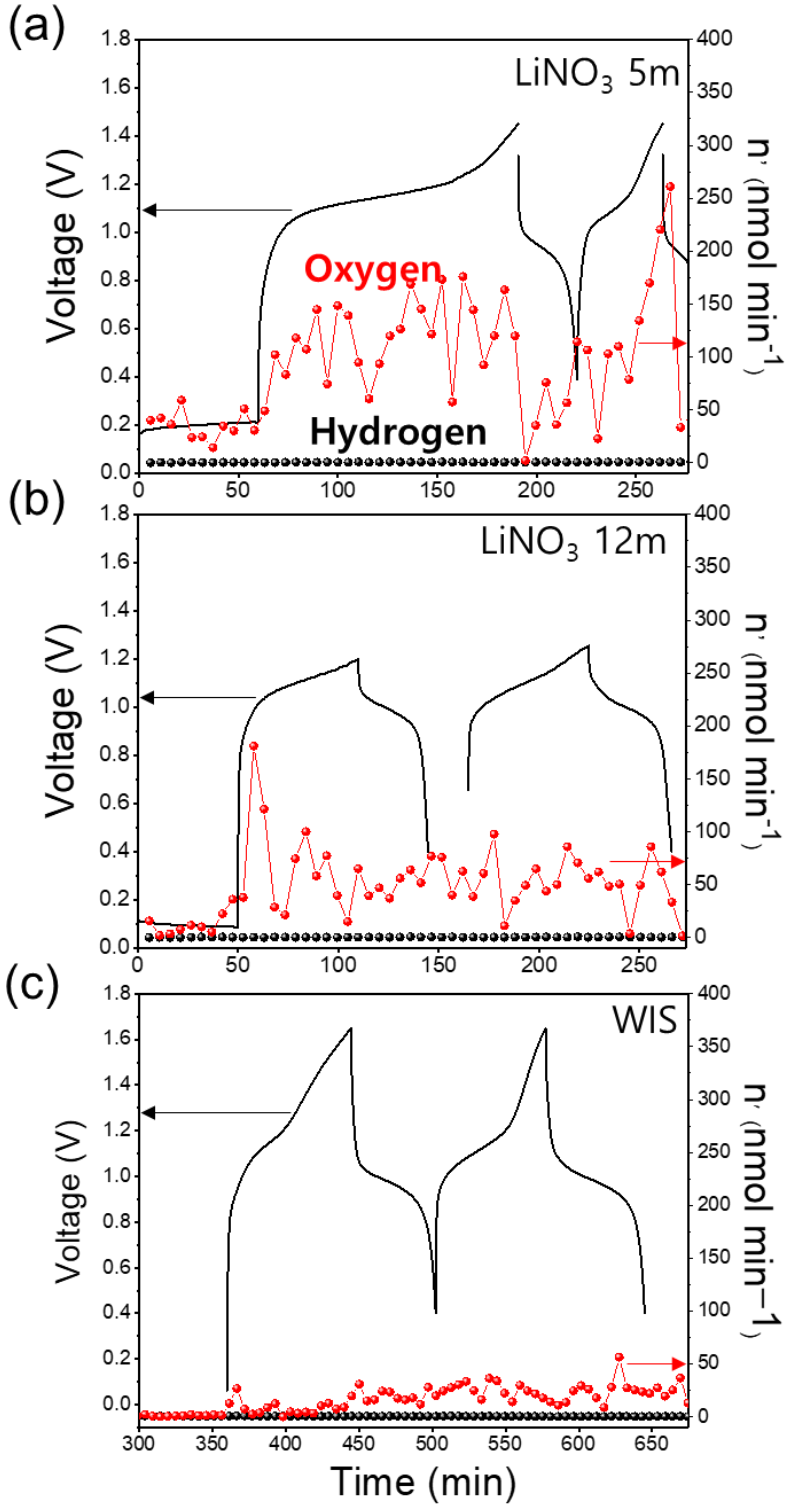

Figure 20 Differential electrochemical mass spectrometry(DEMS) for analyzing amounts of produced oxygen and hydrogen gas of SLMO during initial 2 cycles at 1 C in **(a)** 5 m $LiNO_3$, **(b)** 12 m $LiNO_3$, **(c)** 21 m LiTFSI.

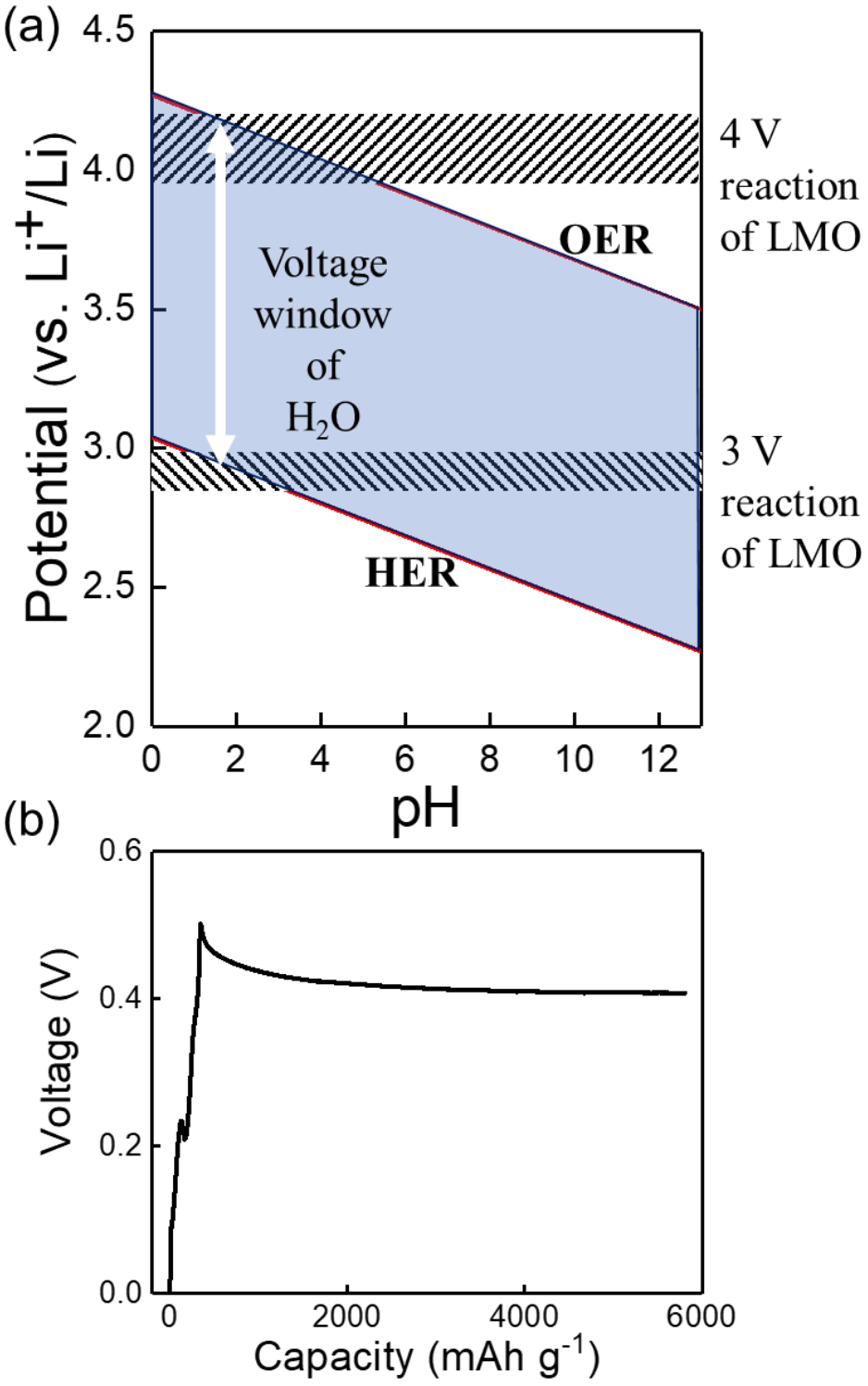

Figure 21 (a) Potential/pH plot which indicates when hydrogen evolution reaction and oxygen evolution reaction were occurred in pure water with various pH range, 0-13. **(b)** Voltage profile of SLMO full cell using 5 m $LiNO_3$ with 0.01 M H_2SO_4 aqueous electrolyte. The cells could not be recharged by side reaction at ~0.4 V.

pure water occurs at 2.62 V_{Li} and OER of pure water occurs at 3.85 V_{Li} which is lower than potential of LMO 4 V reaction (4.0-4.2 V_{Li}). Of course, water decomposition reactions in electrolyte are less reactive than free water, so voltage window of the electrolytes must be wide than free water. From **Figure** 21 a, pH of the electrolyte should be low to suppress OER confirmed in NO_3 aqueous electrolytes by DEMS in this battery system. The **Figure**. 21 b shows that even the pH become low by adding H_2SO_4 solution. The cells with acidic aqueous electrolyte could not be charged by side reaction at ~0.4 cell voltage. When aqueous electrolyte become acid, there are reported problems. High concentration of proton, H+ triggers proton co-insertion, corrosion of current collector and swelling binder material (PVDF) leading to poor cyclability. [11] [12] [4] SUS corrosion was suspected in the cells by the potential of reaction.

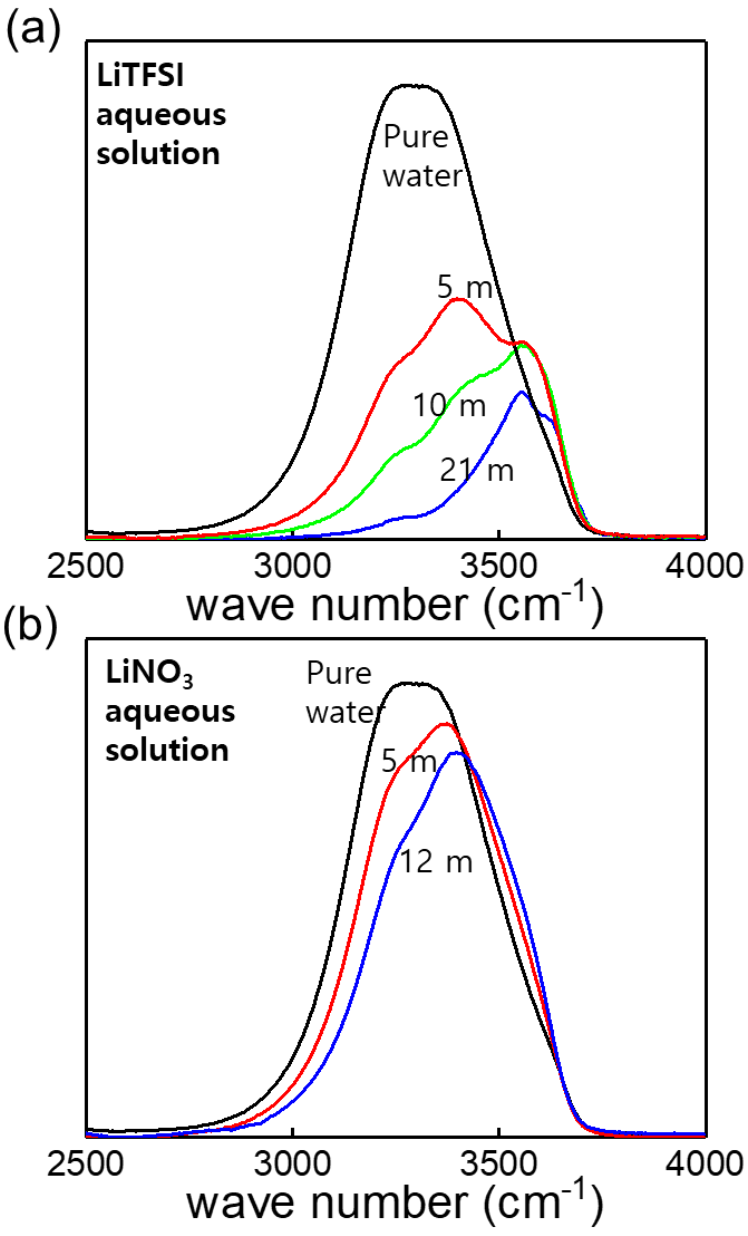

Figure 22 FTIR spectra which of range indicates strength of O-H bond in various concentration of **(a)** LiTFSI aqueous solutions and **(b)** $LiNO_3$ solutions.

From the DEMS data and cell tests, oxygen evolution reaction was verified in charging and discharging with $LiNO_3$ 5m, 12 m electrolytes. The failures of $LiNO_3$ based aqueous electrolytes must have been caused low stability of water molecules. The differences in electrochemical stability and performance are came from the unique property of water in WiSE. The strength of O-H bonds in water can be revealed by Infra-Red spectroscopy. In **Figure** 22, a single broad peak which is from 2700 to 3700 cm^{-1} is observed in pure water. The peak indicates O-H bond and it can be analyzed to 5 different peaks. The peaks are located at 3040, 3220, 3430, 3570, 3630 cm^{-1}. The strongest O-H bond which of peak position is 3630 cm^{-1}indicates that the water molecules free from hydrogen bond. In contrast, the other peaks indicate that the water molecules join hydrogen bond network. The peaks are divided by different interactions with other water molecules. The peaks located at 3570 cm^{-1} is came from O-H bond of water molecules which form three hydrogen bonds. The bonds are composed with two of hydrogen bond as proton donor(D) and one hydrogen bond as proton acceptor(A). From the bond of peak located at 3570 cm^{-1} can be written DDA-OH bond. 3430, 3220, 3040 cm^{-1} peaks are respectively DA-OH, DDAA-OH, DAA-OH bond. [30] The hydrogen bond makes O-H bonds of water molecules weaken. And almost of water molecules when there are no adding salts are participated in hydrogen bond network. From that reason, the broad peak is shown in pure water. In contrast, WiSE shows much narrower peaks than pure water and other dilute solutions. In WiSE, almost water molecules are participated to solvation shell and the water molecules which are in solvation sheaths are not forming hydrogen bond. So, the intensities of peaks which are came from hydrogen bond (3570, 3430, 3220, 3041) are decreased in WiSE and peak positioned at 3630 cm^{-1} get larger proportion than pure water or dilute aqueous solutions. The denser LiTFSI solution has the lesser relative peak intensities of weak O-H bonds which indicates that the water molecules are well included in solvation shell which of center is lithium cation. Comparing with LiTFSI solutions, $LiNO_3$ solutions have much weaker O-H bond. At same time, there are much less decrease of left-side peaks between 12 m $LiNO_3$ and 5 m $LiNO_3$ than between LiTFSI 1 m, 5m, 10m, 21m. That is caused by large charge density which triggers ion pairing of NO_3^-. The stronger O-H bonds make reactivity of water less and consequentially suppress oxygen, hydrogen evolution reaction and from that, one of the reasons why WiSE was successfully recharged unlike the other aqueous electrolyte is revealed.

The activity of water molecules is also important parameter for explaining electrochemical stability of aqueous solution. In **Figure** 23, cyclic voltammetry using stainless steel as working electrode and Pt as counter electrode shows voltage windows of three aqueous solutions. $LiNO_3$ 12 m shows wide voltage window, even the IR showed its weak O-H bond of water molecules. HER and OER in $LiNO_3$ 12 m were occurred at 2.3 V_{Li} and 4.7 V_{Li}. In dense solution, proportion of water molecules on surfaces are decreased and it means that activity of water also decreases. And, that help to prevent water decomposition. $LiNO_3$ 12m still indicates less stability than WiSE in the **Figure** 23 a. In 21 m LiTFSI aqueous electrolyte, HER and OER were occurred at 1.9 V_{Li} and 4.9 V_{Li}. The reaction at 2.9 V indicates SEI layer formation. Unlike the CV test in **Figure** 23 c, in full cell test when using

$LiNO_3$ 12 m aqueous electrolyte, there occurred oxygen evolution reaction which was confirmed by DEMS (**Figure** 20) and suspected by low coulombic efficiency in **Figure** 18 b, 19 d.

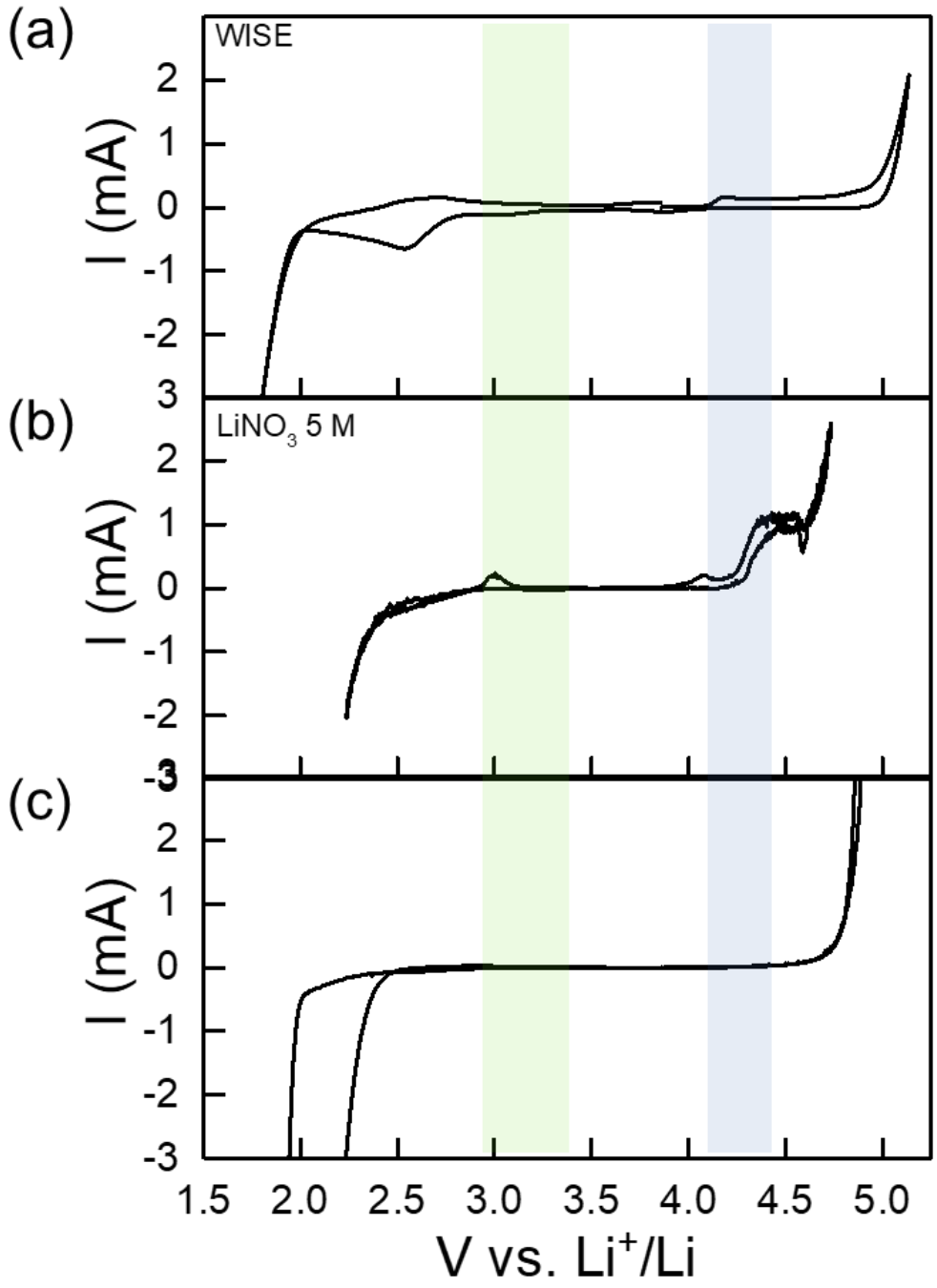

Figure 23 Cyclic voltammetry of **(a)** LiTFSI aqueous solutions and **(b)** $LiNO_3$ solutions. Stainless steel foils and platinum foils, Ag/AgCl in saturated KCl aqueous solution were used as working electrode, counter electrode, reference electrode at scan rate of 10mV s^{-1}. The yellow region and blue region indicate red-ox reactions of LMO.

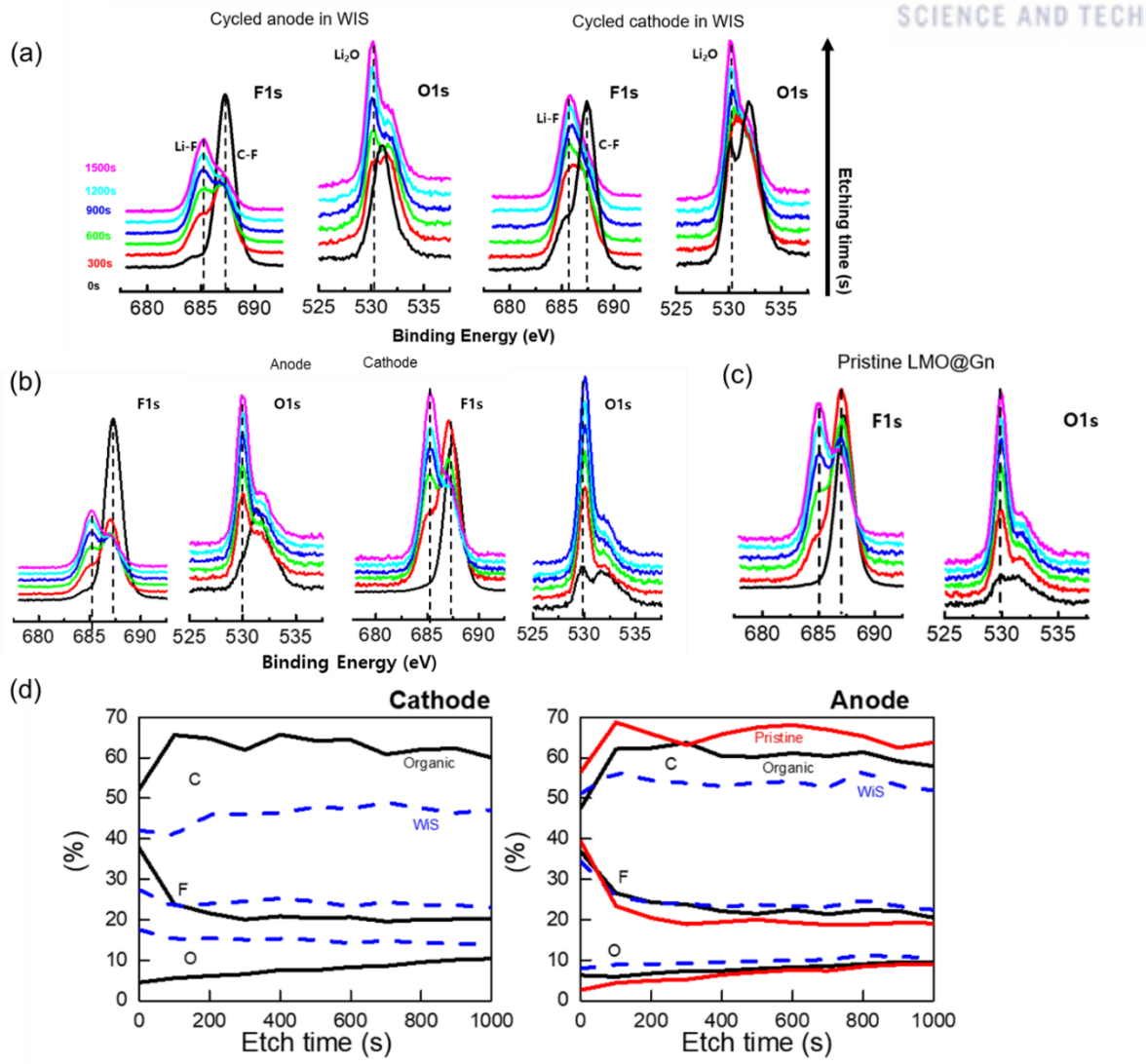

Figure 24 (a)(b)(c) X-ray photoelectron spectroscopy (XPS) F 1s, O 1s spectra of anodes and cathodes of SLMO cells at fully discharged state with Ar^+ etching. The cells were cycled in **(a)** WiS electrolyte, **(b)** Org electrolyte for 20 cycles at 0.2 C. The salts on electrodes of WiSE SLMO were rinsed by washing in DME 3 times. Org SLMO were washed in DMC for 30 minutes. **(c)** XPS spectra of pristine LMO@Gn. **(d)** Depth profiles of the XPS samples which indicates atom composition of samples.

The other reason for suppressed side reactions in WiSE can be a SEI layer formation. It is possible by reduction of solvated TFSI anions complex in super-concentrated solution at higher voltage range (2.4~2.9V vs. Li+/Li) than conventional TFSI anions. The reduction potential is higher than potential of beginning hydrogen evolution reaction (HER) in pH 7, and the SEI layer can exclude water molecules from anode surface effectively. In our battery system, anode cannot cover over TFSI reduction potential range (2.4~2.9V vs. Li+/Li) without overcharging, so stable SEI layer formation in this system is not defined. To confirming that, OCV check after cycling and XPS analysis are practiced.

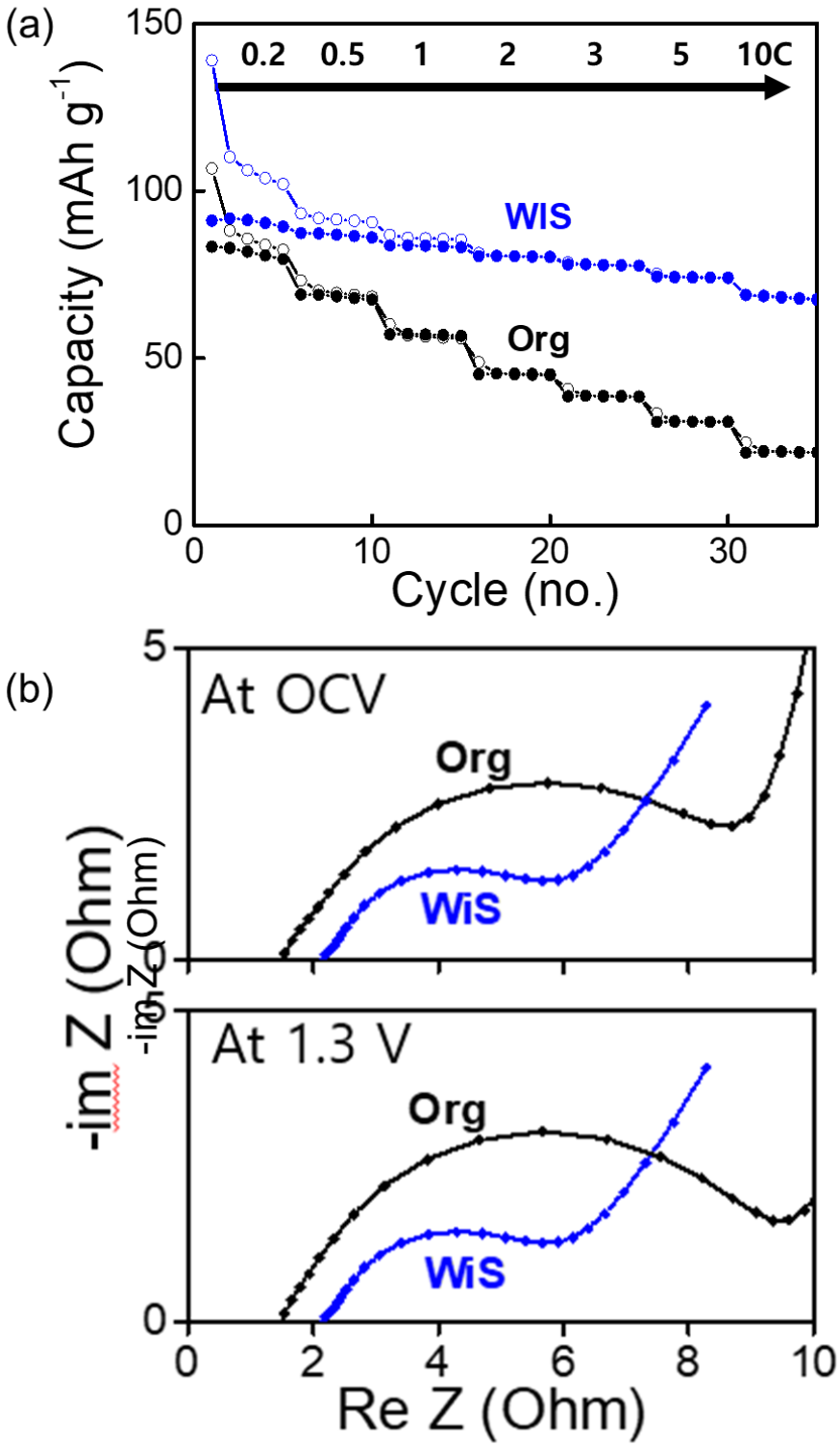

Figure 25 (a) Rate capability test of SLMO full cells using WiS electrolyte and conventional organic electrolyte. The C rate of charging and discharging were 0.2C, 0.5C, 1C, 2C, 3C, 5C and 10C. In low C-rate, **(b)** Nyquist plots of OSLMO and WISE LMO at OCV and 1.3 V, fully charged state.

In our battery system, anode cannot reach TFSI reduction potential range (<2.9V_{Li}) without overcharging, so stable SEI layer formation in this system is not defined.

To figure out certainly, X-ray photoelectron spectroscopy (XPS) analysis with depth profile was used. **Figure** 24 shows F 1s peaks of anodes. There are no big differences between Organic SLMO and WiSE SLMO with different n/p ratio in discharged state. The cells were recharged for 100 cycled at 1C. The peak positioned at 685 eV means Li-F and at ~688 eV may mean F of residual salts in WiSE. There is no big difference of peak position and share of each peak between Pristine LMO@Gn, Organic SLMO and WiSE SLMO. However, depth profiles show different tendency in **Figure** 24 d. Shares of F1s and O1s among Li1s, Al2p, P2p, S2p, C1s, N1s, O1s, Mn2p, F1s are slightly higher in WiSE than pristine LMO@Gn electrode and LMO@Gn cycled in organic electrolyte.

From these results, there might be some SEI layer formation which is not stable as common WiSE using batteries. Reported SEI layer formation was occurred in the voltage range, 2.4 V_{Li} - 2.9 V_{Li} which is lower than 3 V_{Li} of reaction voltage of LMO anode. The image which was obtained by Transmission Electron Microscope (TEM) also support that in **Figure** S4 a. The crystalline layered structure which imply Li-F SEI layer was hard to find in TEM images.

3.3 Kinetics and thermal properties of SLMO battery with WiSE

In **Figure** 25 a, WiSE SLMO coin cell showed slightly higher capacity, 93 mAh/g than using conventional organic electrolyte in 0.2 C rate, 83 mAh g^{-1}. When C rate is higher, the gap of discharging capacity become bigger. The C-rates of charging and discharging were 0.2C, 0.5C, 1C, 2C, 3C, 5C and 10C. SLMO in WiSE shows high capacity and great rate capability. At 10C-rate charge and discharge, the discharge capacity of WiSE SLMO cell conserved to 75.8% of 0.2C discharge capacity. Organic SLMO cell shows only 24% capacity retention in 10 C comparing with first cycle performed in 0.2 C. In **Figure** 25 b, Electrochemical impedance spectroscopy also shows that WiSE SLMO has less charge transference resistance than organic SLMO. The diameter of virtual semicircle when using WiSE is about 4 Ohm and Org is about 9 Ohm at OCV and 1.3 V which is fully charged potential. The small charge transference resistance might be caused by some reasons. One of the reasons is small solvation sheath of WiSE, it makes de-solvation process easy. The other one is a high transference number for lithium of WiSE. Organic electrolyte and WiSE have similar ionic conductivity, ~10mS cm^{-1}. In contrast, transference number for lithium ion (t_{Li}^{+}) of WiSE is much higher than organic electrolyte. t_{Li}^{+} of organic electrolyte is about 0.3. And, because of low charge density of anion and unusual solvation sheath which contains anion, the transference number for lithium ion is 0.7. [21] These properties allow WiSE cells have fast-rechargeability and large capacity which was seemed in **Figure** 25 a.

Figure 26 a showed the discharge capacities of WiSE SLMO, organic SLMO and commercial nickel-metal hydride battery (Ni-MH) at 25° C, 0° C, -20° C and -30° C. The cells were charged at 25° C and then, they were carried and discharged in low temperature chamber. Organic electrolyte is not feasible in low temperature, the discharge specific capacity is close to 0 when temperature is under 0° C. WiSE SLMO battery and Ni-MH battery endured until -20° C with over 60 % of capacity

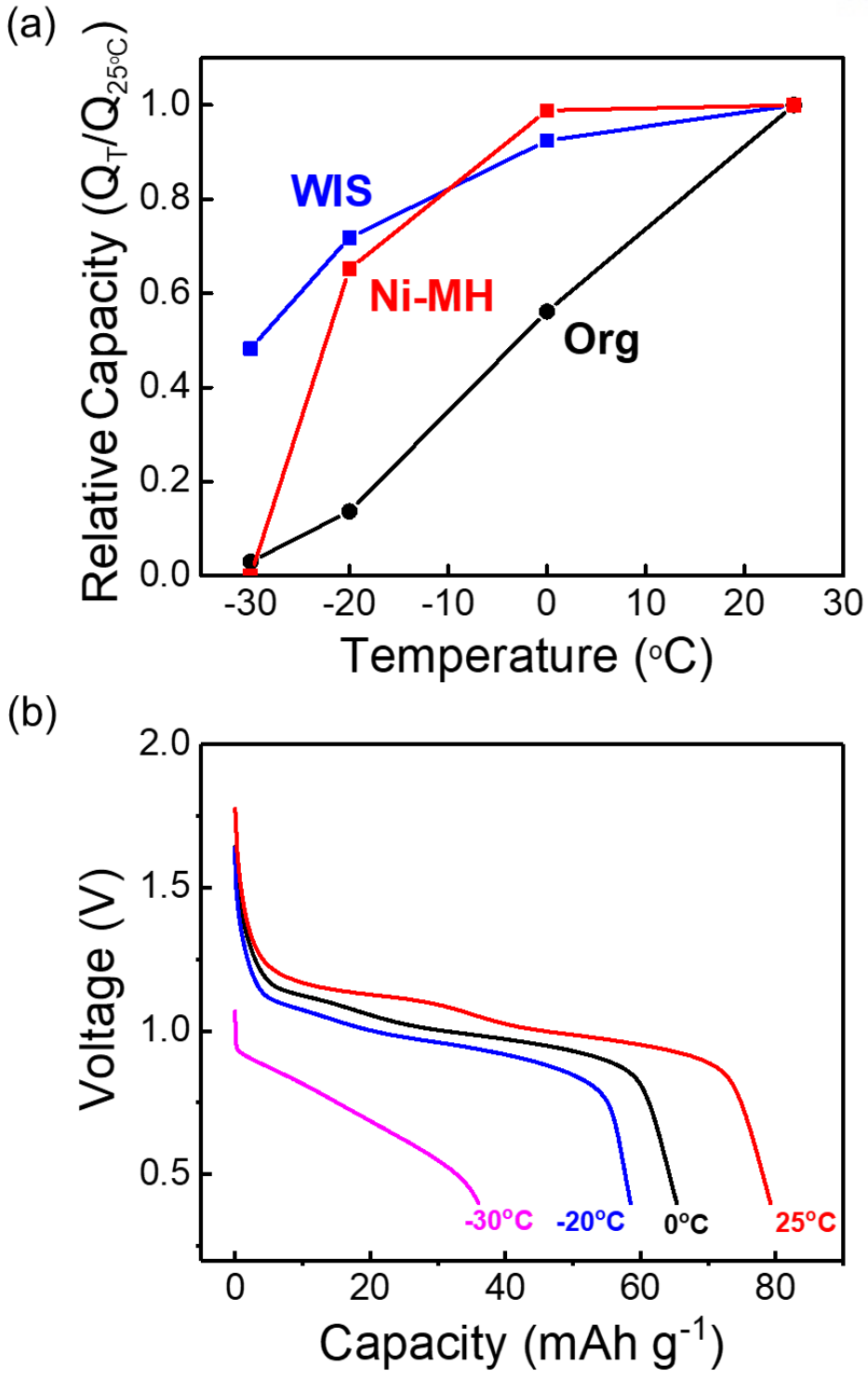

Figure 26 (a) Discharging capacity-temeperature plot for organic SLMO, WiSE SLMO and commercial Ni-MH battery at various temperatures (25, 0, -20, -30°C). Relative capacity is a ratio of the capacity at a specified temperature for capacity at room temperature, 25°C. The marked capacities are discharge capacity at 3rd cycle in 0.2 C. **(b)** Voltage profile of WiSE SLMO in discharging at various temperatures.

retention, but in -30° C the discharge capacity of Ni-MH battery decreased dramatically. Unlikely, WiSE SLMO still realized capacity which was about half of capacity at 25° C. The capacity of WiSE SLMO

is still realized at -30° C. The operation voltages in low temperature were well remained until -20° C in **Figure** 26 b. At -30° C, the operation voltage was about 0.7 V and reaction plateau was not observed, unlikely at -20° C. The rechargeability in low temperature of WiSE SLMO is caused by thermal property of WiSE. From DSC, there were not observed melting point. Instead, T_c of WiSE was observed at -42° C. [10]

4. Conclusion

The realization of SLMO could be done by overcoming two obstacles; Jahn-Teller distortion in LMO anode and water decomposition in dilute traditional aqueous electrolyte. Jahn-Teller distortion in anode was solved by using LMO@Gn electrodes, few layers graphite coated LMO. Water decomposition was suppressed by decreased activity of water molecules in WiSE. Voltage window obtained by cyclic voltammetry could not ensure the rechargeability during cycles. Instead of that, FT-IR spectra about O-H bond was used to predict electrochemical stability and cell performances of each aqueous electrolyte. As prediction, cell performances in WiSE was the great comparing with other aqueous electrolytes.

The characteristics of this SLMO battery system; which are safety, long cycle life, good kinetics, cost efficiency, lower toxicity, high thermal stability is appropriate for large scales of energy storage system from renewable energy generation.

5.Reference

1. Amjad, S.; Neelakrishnan, S.; Rudramoorthy, R., Review of design considerations and technological challenges for successful development and deployment of plug-in hybrid electric vehicles. *Renew. Sust. Energ.* **2010,** *14* (3), 1104-1110.
2. Khaligh, A.; Li, Z. H., Battery, Ultracapacitor, Fuel Cell, and Hybrid Energy Storage Systems for Electric, Hybrid Electric, Fuel Cell, and Plug-In Hybrid Electric Vehicles: State of the Art. *IEEE T. Veh. Technol.* **2010,** *59* (6), 2806-2814.
3. Luo, J. Y.; Cui, W. J.; He, P.; Xia, Y. Y., Raising the cycling stability of aqueous lithium-ion batteries by eliminating oxygen in the electrolyte. *Nat. Chem.* **2010,** *2* (9), 760-5.
4. Kim, H.; Hong, J.; Park, K. Y.; Kim, H.; Kim, S. W.; Kang, K., Aqueous rechargeable Li and Na ion batteries. *Chem. Rev.* **2014,** *114* (23), 11788-827.
5. Khaldi, C.; Mathlouthi, H.; Lamloumi, J., A comparative study, of 1M and 8M KOH electrolyte concentrations, used in Ni–MH batteries. *J. Alloys Compd.* **2009,** *469* (1), 464-471.
6. Ruetschi, P., Aging mechanisms and service life of lead–acid batteries. *J. Power Sources* **2004,** *127* (1), 33-44.
7. Li, W.; Dahn, J. R., Lithium-Ion Cells with Aqueous Electrolytes. *J. Electrochem. Soc.* **1995,** *142* (6), 1742-1746.
8. Jeon, Y.; Noh, H. K.; Song, H.-K., A Lithium-ion Battery Using Partially Lithiated Graphite Anode and Amphi-redox LiMn2O4 Cathode. *Sci. Rep.* **2017,** *7* (1), 14879.
9. Noh, H. K.; Park, H. S.; Jeong, H. Y.; Lee, S. U.; Song, H. K., Doubling the capacity of lithium manganese oxide spinel by a flexible skinny graphitic layer. *Angew. Chem. Int. Ed.* **2014,** *53* (20), 5059-63.
10. Suo, L.; Borodin, O.; Gao, T.; Olguin, M.; Ho, J.; Fan, X.; Luo, C.; Wang, C.; Xu, K., "Water-in-salt" electrolyte enables high-voltage aqueous lithium-ion chemistries. *Science* **2015,** *350* (6263), 938-943.
11. Pei, W.; Hui, Y.; Huaquan, Y., Electrochemical behavior of Li-Mn spinel electrode material in aqueous solution. *J. Power Sources* **1996,** *63* (2), 275-278.
12. Li, W.; McKinnon, W. R.; Dahn, J. R., Lithium Intercalation from Aqueous Solutions. *J. Electrochem. Soc.* **1994,** *141* (9), 2310-2316.
13. Kuhnel, R. S.; Reber, D.; Remhof, A.; Figi, R.; Bleiner, D.; Battaglia, C., "Water-in-salt" electrolytes enable the use of cost-effective aluminum current collectors for aqueous high-voltage batteries. *Chem. Commun.* **2016,** *52* (68), 10435-8.
14. Scrosati, B., History of lithium batteries. *J. Solid State Electr.* **2011,** *15* (7-8), 1623-1630.
15. Winter, M.; Barnett, B.; Xu, K., Before Li Ion Batteries. *Chem. Rev.* **2018,** *118* (23), 11433-11456.
16. Zhao, Y.; Ding, Y.; Li, Y.; Peng, L.; Byon, H. R.; Goodenough, J. B.; Yu, G., A chemistry and material perspective on lithium redox flow batteries towards high-density electrical energy storage. *Chem. Soc. Rev.* **2015,** *44* (22), 7968-96.
17. Li, W.; Dahn, J. R.; Wainwright, D. S., Rechargeable Lithium Batteries with Aqueous Electrolytes. *Science* **1994,** *264* (5162), 1115-1118.
18. Qu, Q.; Fu, L.; Zhan, X.; Samuelis, D.; Maier, J.; Li, L.; Tian, S.; Li, Z.; Wu, Y., Porous LiMn2O4 as cathode material with high power and excellent cycling for aqueous rechargeable lithium batteries. *Energy Environ. Sci.* **2011,** *4* (10), 3985.
19. Tian, L.; Yuan, A. B., Electrochemical performance of nanostructured spinel LiMn2O4 in different aqueous electrolytes. *J. Power Sources* **2009,** *192* (2), 693-697.
20. Yamada, Y.; Usui, K.; Sodeyama, K.; Ko, S.; Tateyama, Y.; Yamada, A., Hydrate-melt electrolytes for high-energy-density aqueous batteries. *Nat. Energy* **2016,** *1* (10).

21. Borodin, O.; Suo, L.; Gobet, M.; Ren, X.; Wang, F.; Faraone, A.; Peng, J.; Olguin, M.; Schroeder, M.; Ding, M. S.; Gobrogge, E.; von Wald Cresce, A.; Munoz, S.; Dura, J. A.; Greenbaum, S.; Wang, C.; Xu, K., Liquid Structure with Nano-Heterogeneity Promotes Cationic Transport in Concentrated Electrolytes. *ACS Nano* **2017,** *11* (10), 10462-10471.
22. Eftekhari, A., High-Energy Aqueous Lithium Batteries. *Adv. Energy Mater.* **2018,** *8* (24), 1801156.
23. Lukatskaya, M. R.; Feldblyum, J. I.; Mackanic, D. G.; Lissel, F.; Michels, D. L.; Cui, Y.; Bao, Z. A., Concentrated mixed cation acetate "water-in-salt" solutions as green and low-cost high voltage electrolytes for aqueous batteries. *Energy Environ. Sci.* **2018,** *11* (10), 2876-2883.
24. Reber, D.; Figi, R.; Kühnel, R.-S.; Battaglia, C., Stability of aqueous electrolytes based on LiFSI and NaFSI. *Electrochim. Acta* **2019,** *321*, 134644.
25. Zheng, J. X.; Tan, G. Y.; Shan, P.; Liu, T. C.; Hu, J. T.; Feng, Y. C.; Yang, L. Y.; Zhang, M. J.; Chen, Z. H.; Lin, Y.; Lu, J.; Neuefeind, J. C.; Ren, Y.; Amine, K.; Wang, L. W.; Xu, K.; Pan, F., Understanding Thermodynamic and Kinetic Contributions in Expanding the Stability Window of Aqueous Electrolytes. *Chem* **2018,** *4* (12), 2872-2882.
26. Yang, C.; Chen, J.; Qing, T.; Fan, X.; Sun, W.; von Cresce, A.; Ding, M. S.; Borodin, O.; Vatamanu, J.; Schroeder, M. A.; Eidson, N.; Wang, C.; Xu, K., 4.0 V Aqueous Li-Ion Batteries. *Joule* **2017,** *1* (1), 122-132.
27. Okumura, T.; Yamaguchi, Y.; Shikano, M.; Kobayashi, H., Further findings of X-ray absorption near-edge structure in lithium manganese spinel oxide using first-principles calculations. *J. Mater. Chem. A* **2014,** *2* (21), 8017-8025.
28. Yang, L.; Takahashi, M.; Wang, B., A study on capacity fading of lithium-ion battery with manganese spinel positive electrode during cycling. *Electrochim. Acta* **2006,** *51* (16), 3228-3234.
29. Li, X. F.; Xu, Y. L.; Wang, C. L., Suppression of Jahn-Teller distortion of spinel LiMn2O4 cathode. *J. Alloys Compd.* **2009,** *479* (1-2), 310-313.
30. Sun, Q., Local statistical interpretation for water structure. *Chem. Phys. Lett.* **2013,** *568*, 90-94.

6. Supporting materials

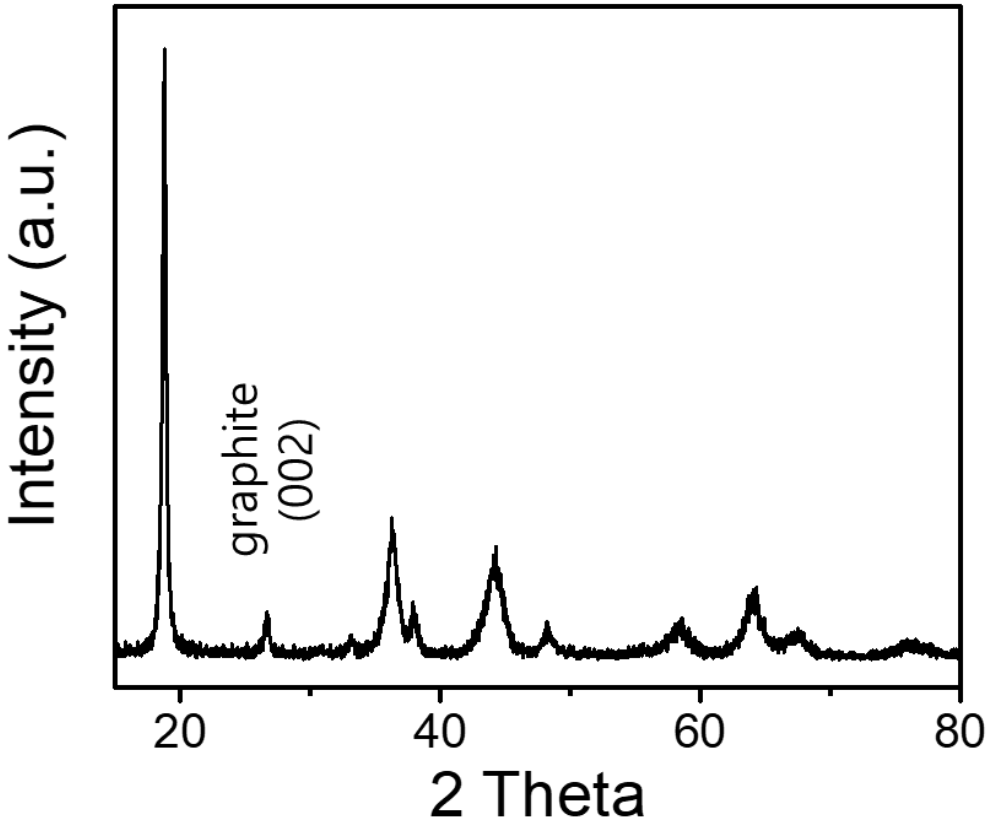

Figure S1. X ray diffraction analysis on synthesized LMO@Gn by high energy ball milling for 6 hours. LMO produced by Aldrich and KS 6 carbon were used for synthesizing.

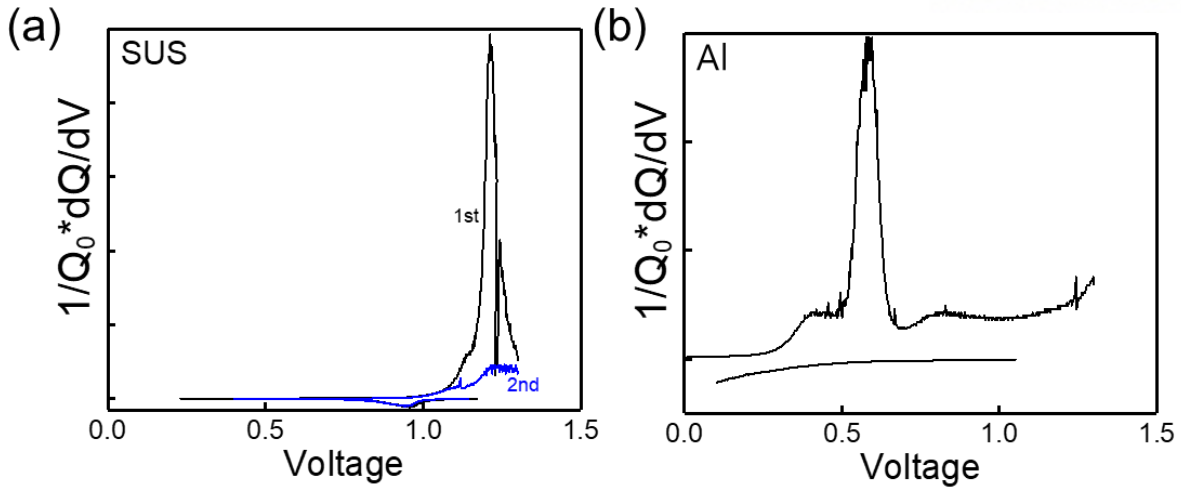

Figure S2. dQ/dV plot versus cell voltage for SLMO battery using 5 m $LiNO_3$ aqueous electrolyte with different current collector. **(a)** Stainless steel and **(b)** aluminum foil was used as current collector, respectively. During cycling, C rates were 1 C.

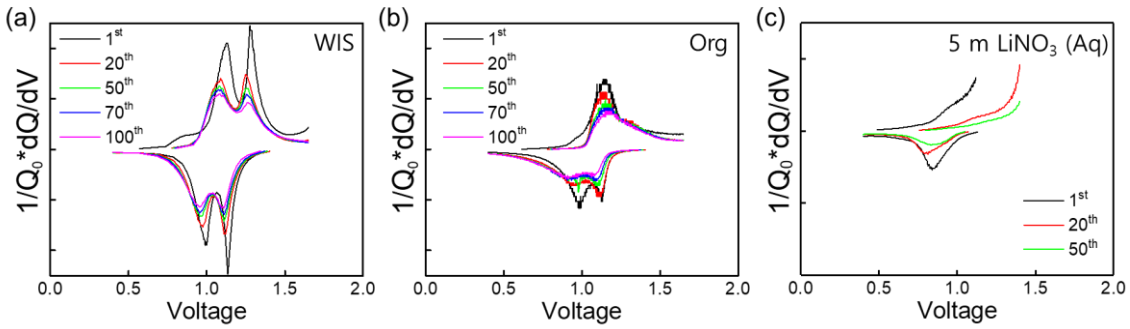

Figure S3. dQ/dV plot versus cell voltage for SLMO batteries using each different electrolyte during 100 cycles at 1 C.

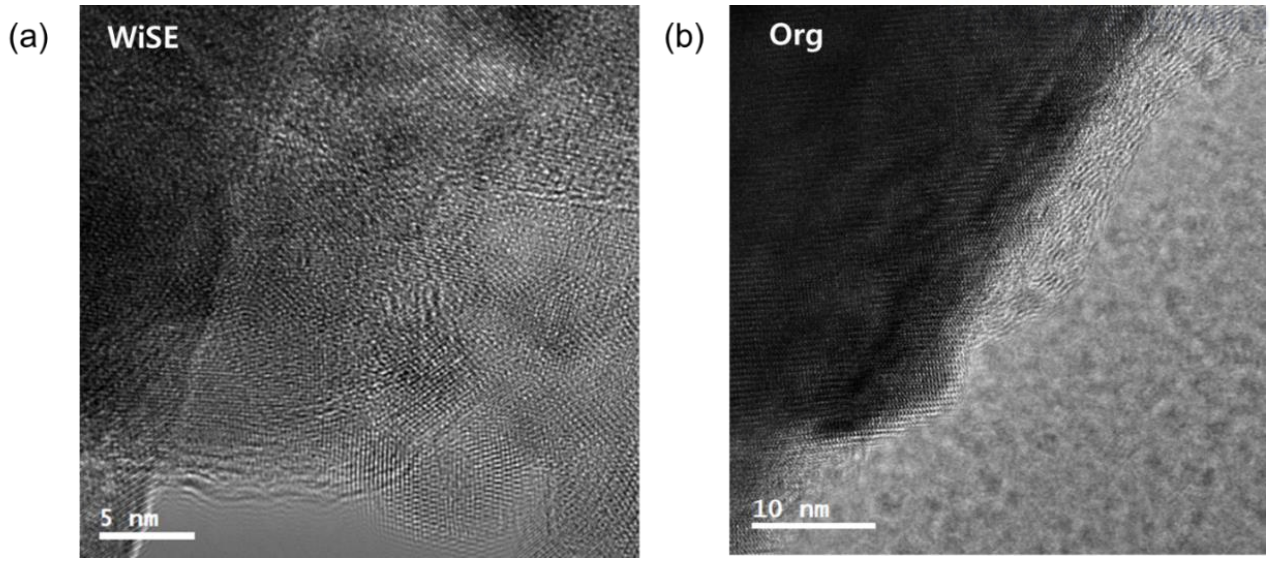

Figure S4. TEM image of LMO@Gn anodes cycled in **(a)** WiSE, **(b)** organic electrolyte.